AAEC/E169

AAEC/E169

AUSTRALIAN ATOMIC ENERGY COMMISSION

RESEARCH ESTABLISHMENT
LUCAS HEIGHTS

METHODS USED TO ANALYSE EXPERIMENTAL DATA OBTAINED WITH THE MOATA TIME OF FLIGHT ANALYSER

by

R. B. TATTERSALL

January 1967

AUSTRALIAN ATOMIC ENERGY COMMISSION

RESEARCH ESTABLISHMENT

LUCAS HEIGHTS

METHODS USED TO ANALYSE EXPERIMENTAL DATA OBTAINED WITH THE MOATA TIME OF FLIGHT ANALYSER

by

R. B. TATTERSALL

ABSTRACT

The theory used to deduce a neutron energy spectrum from counting rate data recorded by the Time of Flight Analyser installed on the reactor MOATA is described in detail. Included are the methods used to calculate energy resolution and slit transmission probabilities assuming either opaque or translucent slit walls. The corrections for energy resolution, dead time, background and air attenuation are also discussed.

CONTENTS

(continued)

CONTENTS (continued)

1. INTRODUCTION

This paper describes in detail the theory used to deduce a neutron energy spectrum from counting rate data recorded in experiments with the Time of Flight Analyser installed on MOATA, the A.A.E.C. Research Establishment's Argonaut type reactor. The aim has been to present the theory in a single report and to attempt to clarify some of the features of transmission by a rotating slit through an alternative approach to the calculations. Basically, however, the theory is similar to that used by Mostovoi et al. (1955), Stone and Slovacek (1956), Larsson et al. (1959), Verbinski and Jarrard (1961), Rocke (Unpublished), and Beckurts and Wirtz (1964).

Computer programmes in Fortran IV (Tattersall Unpublished) have been written to handle the calculations.

2. OUTLINE DESCRIPTION OF THE EXPERIMENTAL ARRANGEMENT

The arrangement of the MOATA Time of Flight Analyser (MOATA chopper) is shown in outline in Figure 1. The rotating slit system releases pulses of neutrons towards the detector twice per revolution of the rotor, and measurements of the flight times over the distance L from the slits to the detector are used to determine the neutron velocities.

The flight times are found by triggering a timing device, Ellis (1964), when the slit opens and stopping it when a neutron is recorded at the detector. The flight times can be divided into a maximum of 512 consecutive channels each of the same width, so that a typical experiment will give up to 512 numbers C_i where:

C_i = number of neutrons per sec arriving at the detector with flight times between t_i and t_{i+1} ,

$(t_{i+1} - t_i) = t_c$ = time channel width.

This report gives the relation between C_i and the neutron spectrum $\phi(E)$ in the reactor at the base of the probe hole shown in Figure 1.

3. TRANSMISSION OF A SLIT SYSTEM

Consider first the case of a chopper with a stationary rotor with a single slit which is fully open, and assume initially that the material defining the slit is completely opaque to neutrons. Since the length of the slit is short compared with the slit source and slit detector distances (15cm compared with 150 cm and 800 cm for the MOATA chopper) its length can be ignored, except in the detailed calculation of its transmission probability (see Appendices II, III and IV). The system being considered is shown in Figure 2.

The source plane is the base of the probe hole (Figure 1) and the area from which the detector receives neutrons is determined by the heights and widths of the detector and slit as shown by the lines CAC' and $DA'D'$ in Figure 2.

Put L' = distance source to slit,

L = distance slit to detector,

h = height of the slit (AA'),

h_d = height of the detector (CD),

h_s = height of the source ($C'D'$);

then from the similar triangles ABC, $AB'C'$ of Figure 2:

$$\frac{h_s - h}{2}\ \frac{1}{L'} = \frac{h_d + h}{2}\ \frac{1}{L} \quad ,$$

hence

$$h_s = h + \frac{L'}{L}(h_d + h) \quad . \qquad 3.1$$

A similar relation will hold for the widths of the source, slit, and detector.

Provided size of the base of the probe hole exceeds the source size, h_s defined by the lines CAC' and DA'D' of Figure 2, the area of the source from which a point X on the detector receives neutrons will be constant (Figure 3). This area will be (Figure 3):

$$A = A_s \left(\frac{L + L'}{L}\right)^2 ,$$

where A_s = area of slit.

It is therefore possible to account for the effect of the slit by assuming that the detector is receiving neutrons from a point source of strength:

$$S = \frac{\phi}{4} A$$

$$= \frac{\phi}{4} A_s \left(\frac{L + L'}{L}\right)^2$$

where

ϕ = neutron flux at the source plane (assumed isotropic and constant throughout a region round the base of the probe hole).

The number of neutrons crossing the detector per second is therefore:

$$n = S \frac{A_d}{2\pi(L + L')^2}$$

$$= \frac{A_s A_d \phi}{8\pi L^2} \qquad 3.2$$

where A_d = area of the detector.

In Appendix I an alternative derivation of Equation 3.2 is given which enables the effect of a non-uniform source to be calculated.

As the rotor rotates, the height of the neutron beam transmitted varies between zero and some maximum which depends on the energy of the neutrons concerned. Choose time zero as the time when the slit is horizontal, (that is, fully open), and put:

$h_b(E,t)$ = height of a beam of neutrons of energy E which crossed the vertical plane through the axis of rotation of the rotor at time t.

$n(E,t)$ = number of neutrons per sec travelling towards the detector per unit E and t.

ω = angular velocity of the rotor.

From Equation 3.2:

$$n(E,t) = \frac{A_s A_d \phi(E)}{8\pi L^2} \frac{h_b(E,t)}{h}$$

Since $n(E,t)$ is periodic, consisting of identical neutron bursts occurring twice per revolution of the rotor, the total rate at which neutrons arrive at the detector is the product of the integral over one burst and the burst frequency. We accordingly replace the above expression by:

$$n(E,t) = \frac{\omega}{\pi} \frac{A_s A_d \phi(E)}{8\pi L^2} \frac{h_b(E,t)}{h}$$

$$= \frac{\omega A_s A_d \phi(E)}{8\pi L^2} \frac{h_b(E,t)}{h} \qquad 3.3$$

where only the non–zero values of $h_b(E,t)$ near $t = 0$ are considered in any time integration. The factor $h_b(E,t)/h$ is the differential neutron transmission probability per unit slit height.

The simplest form of $h_b(E,t)$ is for neutrons of infinite velocity since there is no rotation of the rotor whilst they are traversing it. In this case the beam height rises linearly to the slit height h and then falls linearly.

Put

r = rotor radius

$2r$ = length of slit.

The slit starts to open (see Figure 4) at $t = -h/2\omega r$ and closes at $t = h/2\omega r$ so that:

$$h_b(\infty,t) = h\left(1 - \frac{2\omega r}{h}|t|\right) \quad \text{for} \quad |t| < h/2\omega r \qquad 3.4$$

$$= 0 \text{ otherwise.}$$

Thus the number of infinite velocity neutrons per second travelling towards the detector is, from Equations 3.3 and 3.4,

$$N_T(\infty) = \frac{\omega A_s A_d \phi(\infty)}{8\pi^2 L^2} \int_{-h/2\omega r}^{h/2\omega r} \left(1 - \frac{2\omega r}{h}|t|\right) dt$$

$$= \frac{\omega A_s A_d \phi(\infty)}{8\pi^2 L^2} \cdot \frac{h}{2\omega r}$$

The factor $h/2\omega r$ is the total transmission probability per burst for neutrons of infinite velocity, and it is convenient to define other transmission probabilities relative to this. Denoting the relative differential transmission probability by $\tau_1(E,t)$ we have:

$$\tau_1(E,t) = \frac{h_b(E,t)}{h} \Big/ \frac{h}{2\omega r} \quad , \qquad 3.5$$

and substituting in (3.3):

$$n(E,t) = \frac{A_s A_d h \phi(E) \tau_1(E,t)}{16\pi^2 L^2 r} \quad . \qquad 3.6$$

We also define the total relative transmission probability per burst:

$$\tau(E) = \int \tau_1(E,t)\, dt \quad . \qquad 3.7$$

where the integral is over the whole of one burst.

In the case where the material forming the slit is not opaque to neutrons, similar expressions to the above can be obtained. Using primed quantities to denote functions applicable when the slit walls are translucent, we put:

c = height of neutron above rotor axis

ℓ = neutron path length in rotor material

Σ = total macroscopic cross section of rotor material

$p'(E,t,c)$ = probability of transmission of neutron

$$= \exp(-\Sigma\ell) \, .$$

The effective height of the slit analogous to $h_b(E,t)$ of the above relations is

$$h_b'(E,t) = \int p'(E,t,c)\,dc \qquad 3.8$$

where the integral is over all values of c. In practice $p'(E,t,c)$ is non-zero over a range a little more than the height of the slit.

The analogous relations to (3.5), (3.6), and (3.7) are:

$$\tau_1'(E,t) = \frac{2\omega r}{h^2} \int p'(E,t,c)\,dc \qquad 3.9$$

$$\tau'(E) = \int \tau_1'(E,t)\,dt \qquad 3.10$$

$$n'(E,t) = \frac{A_s A_d\, h\, \phi(E)\, \tau_1'(E,t)}{16\pi^2 L^2 r} \qquad 3.11$$

The detailed derivations of τ_1, τ, τ_1', τ' are given in Appendices II, III and IV.

4. CHANNEL COUNTS

Since a neutron which hits the detector at a time t' passed the slit axis at a time:

$$t = t' - \frac{L}{v} \quad ,$$

where L = rotor to detector flight path

v = neutron velocity,

the counting rate of the detector at a time t' will be:

$$C(E,t') = n\left(E, t' - \frac{L}{v}\right) \epsilon(E)$$

where $\epsilon(E)$ = counting efficiency of detector for neutrons of energy E.

As noted in Section 2 the detector count rate is measured in a set of time channels of equal width. For channel i extending from time t_i' to t_{i+1}' after the slits crossed the horizontal, the total count rate from neutrons of all energies will be

$$C_i = \int_{E=0}^{\infty} \int_{t'=t_i'}^{t_{i+1}'} n\left(E, t' - \frac{L}{v}\right) \epsilon(E)\, dE\, dt'$$

$$= \frac{A_s A_d\, h}{16\pi^2 L^2 r} \iint \phi(E)\, \epsilon(E)\, \tau_1\left(E, t' - \frac{L}{v}\right) dE\, dt' \qquad 4.1$$

This double integral can be evaluated analytically subject to certain approximations. The function $\tau_1(E,t)$ of Equation 3.5 does not vary strongly with E, but is non-zero only for a small range of t (approximately for $-h/2\omega r < t < h/2\omega r$). Accordingly the energy dependence of $\tau_1(E, t'-L/v)$ arises almost entirely from its second argument and it is apparent that only a small energy range of neutrons is detected in the i^{th} counting channel. This range is given approximately by the velocity range defined by:

$$-h/2\omega r < t' - L/v < h/2\omega r$$

where the range of t' is given by the counting channel time boundaries. Hence this velocity range is given by:

$$\frac{L}{t_{i+1}' - \frac{h}{2\omega r}} < v < \frac{L}{t_i' + \frac{h}{2\omega r}}$$

If we put in Equation 4.1:

$$t = t' - L/v$$

$$v = L/(t' - t)$$

$$E = k/(t' - t)^2 \quad (k \text{ is a constant})$$

$$dE = \frac{2k}{(t' - t)^2}\, dt$$

$$= \frac{2Ev}{L}\, dt \quad ,$$

the integral with respect to E becomes:

$$I = \int_0^\infty \phi(E)\, \epsilon(E)\, \tau_1(E, t' - L/v)\, dE$$

$$= \frac{2}{L} \int_{-\infty}^{t'} v\, E\, \phi(E)\, \epsilon(E)\, \tau_1(E, t)\, dt \quad .$$

As already noted $\tau_1(E,t)$ is non-zero only over a small range of t. This range does not exceed $-h/2\omega r < t < h/2\omega r$ (see Appendix III), so if for the whole of the counting channel concerned we have:

$$t' > h/2\omega r \quad ,$$

$$I = \frac{2}{L} \int_{-h/2\omega r}^{h/2\omega r} v\, E\, \phi(E)\, \epsilon(E)\, \tau_1(E, t)\, dt \quad . \qquad 4.2$$

Since $\tau_1(E,t)$ is symmetrical about $t = 0$, then provided the quantity $v\, E\, \phi(E)\, \epsilon(E)$ is constant or varies linearly with t over the integration range (note that E is a function of t for a given t') it is possible to replace E and v with their values E_o and v_o at the centre, $t = 0$, of the integration range and obtain:

$$I = \frac{2\, v_o\, E_o\, \phi(E_o)\, \epsilon(E_o)}{L} \int \tau_1(E_o, t)\, dt$$

$$= \frac{2 v_o\, E_o\, \phi(E_o)\, \epsilon(E_o)\, \tau(E_o)}{L} \quad .$$

E_o and v_o are functions of t' so, again assuming that I is constant or varies linearly with t', we perform the integration with respect to t' in Equation 4.1 by replacing the variable I with its value at the centre T_i of the t' integration range. Thus we have:

$$T_i = 0.5\, (t'_{i+1} + t'_i)$$

$$v_i = L/T_i$$

E_i = energy corresponding to v_i ,

and

$$C_i = \frac{A_s\, A_d\, h}{16 \pi^2 L^2 r} \cdot \frac{2 v_i\, E_i\, \phi(E_i)\, \epsilon(E_i)\, \tau(E_i)}{L} \int_{t'_i}^{t'_{i+1}} dt'$$

$$= \frac{A_s\, A_d\, h\, E_i\, \phi(E_i)\, \epsilon(E_i)\, \tau(E_i)\, t_c}{8 \pi^2 L^2 r\, T_i} \quad , \qquad 4.3$$

where $t_c = t'_{i+1} - t'_i$ is the time channel width.

The approximations made in deriving Equation 4.3 are quite good. The first one ($t' > h/2\omega r$, Equation 4.2) implies that the lower time boundary of the first channel must be greater than $h/2\omega r$. This means that the slit must be closed for infinite velocity neutrons before time measurements are started. The second main assumption concerning the linearity of certain expressions also holds quite well. There are two cases:

(1) High Energy (that is, early time channels): In this case we often have:

(a) $E\phi(E)$ = constant

(b) $\epsilon(E) \propto 1/v$

(c) $\tau(E)$ = constant.

This means that $vE\phi(E)\epsilon(E)$ is constant which is the required approximation.

(2) Low Energy (that is, late time channels): In this case the energy or velocity widths of the time channels are small because:

$$E \propto 1/t^2 \qquad v \propto 1/t$$

$$dE \propto -\frac{dt}{t^2} \qquad dv \propto -\frac{dt}{t^3}$$

so the energy and velocity intervals fall rapidly with rising t. Consequently $vE\phi(E)\epsilon(E)$ is again constant across a channel because of the small energy range involved.

5. MULTIPLE SLITS

In the preceding discussion we have considered a rotor with a single slit passing symmetrically through the rotor axis. In practice several slits parallel to each other are normally used, and the effect of this is now considered.

Consider first a single off-axis slit. Since neutrons pass through the slit for only a very small rotation about the rotor axis (from approximately $\theta = -h/2r$ to $\theta = +h/2r$ (see Figure 4)), the translational motion of the centre of the slit will be very small. To a very good approximation, the slit motion will be a pure rotation like the axially aligned slit, so the transmitted burst will have exactly the shape discussed already (see also Appendix II).

Figure 5 illustrates the effect of multiple slits on source size. The detector views a different area of the source (UV, YZ) through each slit, and the total area viewed is determined by the overall height of the slit system.

The flight axes ABC, AB'C' for the different slits are slightly inclined to each other so that the slits will be fully open for neutron transmission at slightly different rotor angles. Thus although the shape of the transmitted burst is the same for both slits, the bursts occur at a slightly different time. However, this time difference is usually small compared to the burst width, so that its only effect is a slight worsening of the chopper resolution. This is discussed further in Section 6 and in Appendix VI.

It is concluded that the transmission from a multiple slit system is just that from a single slit multiplied by the number of slits, so that for a system containing N slits Equations 4.1 and 4.3 become:

$$C_i = \frac{N A_s A_d h}{16\pi^2 L^2 r} \iint \phi(E)\,\epsilon(E)\,\tau_i(E, t'-L/v)\,dE\,dt' \qquad 5.1$$

$$C_i = \frac{N A_s A_d h E_i \phi(E_i)\,\epsilon(E_i)\,\tau(E_i)\,t_c}{8\pi^2 L^2 r\, T_i} \qquad 5.2$$

The height of the source viewed by the detector is determined by Equation 3.1 with h replaced by the overall height of the slit system. There is also a small effect on the chopper resolution as discussed below.

6. RESOLUTION

6.1 Introduction

The accuracy to which neutron energy can be determined by a chopper measurement depends on the flight path used and the uncertainty in the measurement of flight time. Denoting flight path and flight time by L and T respectively, we can express neutron velocity and energy as:

$$v = L/T \qquad 6.1$$

$$E = k v^2 \quad (k \text{ is a constant})$$

$$= k L^2/T^2 \qquad 6.2$$

$$\Delta E = -2k L^2 \Delta T/T^3 \qquad 6.3$$

$$\frac{\Delta E}{E} = -\frac{2\Delta T}{T} \qquad 6.4$$

For a criterion of performance an expression for ΔE at a given energy is required and since T for a given E depends on the flight path, Equations 6.1 and 6.4 are combined to give:

$$\Delta E = -2E v \frac{\Delta T}{L} \qquad 6.5$$

The resolution of a chopper is therefore determined by the ratio of flight time uncertainty to flight path and is usually expressed in units of microseconds per metre.

Since the counting rate in a measurement is inversely proportional to L^2 (Equations 4.1, 4.3, 5.1, 5.2) there is a limit to which L can usefully be increased to improve resolution.

6.2 Contributions to Flight Time Uncertainty

The uncertainty in the neutron flight time in a chopper measurement arises from the following sources:

(i) Time width of the neutron burst transmitted by the slits.

(ii) Time taken for the neutron beam to be swept across the detector.

(iii) Time difference between the peaks of the bursts from different slits.

(iv) Uncertainty in the time of detection (the time channel width).

(v) Uncertainty in the depth of neutron penetration into the detector before absorption.

The uncertainty of the neutron flight time will be expressed in terms of its variance V_T. In general for a variable x with a probability distribution f(x), the variance of x about its mean value $\bar{x}$ is given by:

$$V = \frac{\int_{-\infty}^{\infty} (x-\bar{x})^2 f(x)\,dx}{\int_{-\infty}^{\infty} f(x)\,dx} \qquad 6.6$$

where

$$\bar{x} = \frac{\int_{-\infty}^{\infty} x f(x)\,dx}{\int_{-\infty}^{\infty} f(x)\,dx} \qquad 6.7$$

Thus to find V_T it is necessary to know something about the probability distributions of the above contributions to the timing uncertainties.

For the neutron burst transmitted by slit, the probability distribution is just $\tau_1(E,t)$ or $\tau_1'(E,t)$ which are given in Appendices III or IV according to whether or not the slit walls are opaque to neutrons. If the walls are opaque, it can be seen from Figure 17 that a close approximation to $\tau_1(E,t)$ is a triangle of base width $2T_b$ where:

$$\begin{aligned} T_b &= 0 && \beta > 1 \\ &= \frac{4s\beta}{\omega r}\left(\frac{1}{\sqrt{\beta}} - 1\right) && \frac{1}{4} < \beta < 1 \\ &= s/\omega r && 0 < \beta < \frac{1}{4} \end{aligned} \qquad 6.8$$

This approximation is adequate for variance calculations.

For translucent slit walls the function $\tau_1'(E,t)$ is more complicated, but following the approximation given in Appendix V, the above triangular distribution can still be used provided r is replaced by $r' = (r - 1/\Sigma)$ and β by β' (see Appendix V Equations 2 and 3).

The analysis which gave $\tau_1(E,t)$ and $\tau_1'(E,t)$ assumed a point detector. For a detector of finite height the analysis holds for each point on the detector except that each point has its own zero time, that is, the time when the slit is pointing directly at it. The burst width is therefore increased by a time $2T_s$ which the slit takes to sweep across the detector. Figure 6 shows that:

$$T_s = \frac{h_d}{2\omega L}$$

The presence of multiple slits with a distance H between the centre lines of the outermost slits further increases the burst width because (see Figure 7) the burst from the top slit sweeps the detector at a time $H/\omega L$ before that from the bottom slit. The total burst width is therefore increased by the time $2T_m$ where:

$$T_m = \frac{H}{2\omega L}$$

The final burst shapes obtained when finite detector height and slit multiplicity are considered are discussed in Appendix VI where it is concluded that the distributions shown in Figure 8 are reasonable approximations for the purpose of variance calculations. There are two cases to be considered:

(i) $T_s < (T_b + T_m)$ (small detector): Burst shape is triangular with a base width of $2(T_s + T_b + T_m)$. A mathematical representation is:

$$\begin{aligned} f(t) &= 1 - \frac{|t|}{T_s + T_b + T_m} && 0 < |t| < (T_s + T_b + T_m) \\ &= 0 && |t| > (T_s + T_b + T_m) \end{aligned}$$

(ii) $T_s > (T_b + T_m)$ (large detector): Burst rises linearly over a period $2(T_b + T_m)$, is constant for a time $2(T_s - T_b - T_m)$, and falls linearly to zero over a time $2(T_b + T_m)$. A mathematical representation is:

$$\begin{aligned} f(t) &= 1 && 0 < |t| < (T_s - T_b - T_m) \\ &= 1 - \frac{|t| - (T_s - T_b - T_m)}{2(T_b + T_m)} && (T_s - T_b - T_m) < |t| < (T_s + T_b + T_m) \\ &= 0 && |t| > (T_s + T_b + T_m) \end{aligned}$$

In both cases the total width of the burst is $2(T_s + T_b + T_m)$ and it is symmetrical about $t = 0$, so the mean value of t is zero. The variances of t are therefore given by:

$$V_B = \frac{\int_{-\infty}^{\infty} t^2 f(t)\,dt}{\int_{-\infty}^{\infty} f(t)\,dt}$$

$$= \frac{1}{6}(T_s + T_b + T_m)^2 \qquad T_s < (T_b + T_m)$$

$$= \frac{1}{3}\{T_s^2 + (T_b + T_m)^2\} \qquad T_s > (T_b + T_m) \quad . \qquad 6.9$$

The uncertainty in the time of detection arises mainly from the width t_c of the timing channels, but there are also possibilities of errors in the location of time zero and in the time scale. Time zero occurs when the slit system is horizontal and this can be located quite readily by the method described in Section 11 to about 10 per cent. of the channel width. This represents an appreciable error only for the first few channels. Errors in the time scale are negligible since this is set by a crystal controlled 2Mc/s oscillator. However, the timing is achieved by counting pulses at a frequency of 2Mc/s from this oscillator and since this is free running there will be an uncertainty of up to 0.5 μs in the time interval between a start pulse and the occurrence of the first timing pulse. The minimum channel width used is 4μs so this error is again negligible, except in the first few channels. The probability distribution of detection times is therefore of width t_c and is square in shape, being zero outside the timing channel and unity inside. Hence for timing channel i which extends between flight times $(T_i - 0.5\,t_c)$ and $(T_i + 0.5\,t_c)$ the mean flight time is T_i and the variance about this is, from Equation 6.6:

$$V_C = \frac{\int_{(T_i - 0.5\,t_c)}^{(T_i + 0.5\,t_c)} (t - T_i)^2\,dt}{\int_{(T_i - 0.5\,t_c)}^{(T_i + 0.5\,t_c)} dt} = \frac{t_c^2}{12} \qquad 6.10$$

The uncertainty in the depth of penetration of a neutron into the detector leads to a flight path uncertainty ΔL which is equivalent to a flight time uncertainty $\Delta L/v$. The probability of a neutron penetrating a depth x into the detector is:

$$f(x) = e^{-\Sigma_d x}$$

where Σ_d is the macroscopic absorption cross section of the detector. If it is assumed that the detector is of a uniform thickness ℓ_d then the mean depth of penetration into the detector is:

$$\bar{x} = \frac{\int_0^{\ell_d} x\, e^{-\Sigma_d x}\,dx}{\int_0^{\ell_d} e^{-\Sigma_d x}\,dx}$$

$$= \frac{1}{\Sigma_d}\left[1 - \frac{\Sigma_d \ell_d\, e^{-\Sigma_d \ell_d}}{1 - e^{-\Sigma_d \ell_d}}\right]$$

and the variance about $\bar{x}$ is

$$V_x = \frac{\int_0^{\ell_d} (x - \bar{x})^2\, e^{-\Sigma_d x}\,dx}{\int_0^{\ell_d} e^{-\Sigma_d x}\,dx}$$

$$= \frac{1}{\Sigma_d}\left[\Sigma_d \ell_d \bar{x} + 2\bar{x} - \Sigma_d \bar{x}^2 - \ell_d\right] \quad . \qquad 6.11$$

and the corresponding flight time variance is:

$$V_F = V_X / v_i^2 = V_X \, T_i^2 / L^2 \quad . \qquad 6.12$$

There are two limiting cases of Equation 6.11 which are of interest. The first is for a 'thin' detector that is one with small $\Sigma_d \ell_d$. In this case, expanding $\exp(-\Sigma_d \ell_d)$ gives:

$$\bar{x} = \frac{\ell_d}{2} - \frac{1}{12}\Sigma \ell_d^2 \simeq \frac{\ell_d}{2} \qquad \text{for small } \Sigma_d \ell_d$$

$$V_X = \ell^2/12 \quad ;$$

(note that the term in $\Sigma \ell_d^2$ in $\bar{x}$ is essential to calculate V_X correctly). These are the expected results because neutron attenuation by a thin counter is negligible, so there is constant probability of absorption across the counter. The mean depth of penetration is therefore just half the total counter depth and the variance is that for a square probability distribution (compare with Equation 6.10).

For a thick counter that is, one with very large Σ_d, we find:

$$\left.\begin{aligned} \bar{x} &= 1/\Sigma_d \\ V_X &= 1/\Sigma_d^2 \end{aligned}\right\} \qquad \text{for large } \Sigma_d \quad .$$

This means that all neutrons are absorbed close to the surface of the detector.

Since Σ_d is energy dependent, so also is the mean depth of penetration into the detector. If a counter with a high efficiency at low energy is used, the thick counter approximation will hold and low energy neutrons will be absorbed near the counter surface. At high energies the thin approximation will hold so that there will be a change of flight path of half the counter thickness.

Having obtained the above independent contributions to the variance of the flight time, the total variance V_T is just the sum of these, that is (see Equations 6.9, 6.10, 6.12):

$$V_T = V_B + V_C + V_F \quad .$$

The flight time of neutrons recorded in channel i is therefore $(T_i \pm \Delta T_i)$, where:

$$\Delta T_i = \sqrt{V_T} \quad .$$

where V_T is the variance for channel i.

It is usual to express chopper resolution as a total energy spread in a channel, that is, as the energy spread corresponding to $2\Delta T_i$; hence from Equation 6.5 the resolution is:

$$R = \frac{2\Delta T_i}{L} \quad (\mu s/m) \quad .$$

For the MOATA chopper, the principal contributions to the flight time variance are V_B and V_C, the burst width T_b from the slit being the major contribution to V_B. The contribution of the change of flight path with energy can normally be ignored. Typical figures for resolution are as follows:

MOATA Chopper Resolution (L = 800cm)

Rotor Speed (r.p.m.)	Resolution (μs/m)
1800	8
3600	4
7200	2
14400	1

7. RESOLUTION CORRECTION

The relation between channel counts and flux (Equations 4.3, 5.2) obtained in Sections 4 and 5 depended on the assumption that the quantity $v\,E\,\phi(E)\,\epsilon\,(E)$ varied linearly across a counting channel. This assumption can break down, for example, if $E\,\phi(E)$ varies strongly with energy, as it may do if a strong resonance absorber is present, or if a counting channel covers a wide energy range, as in the case of the first few channels. To handle such cases a more accurate integration of Equations 4.1 or 5.1 must be made.

One way of treating the problem is to assume that at least an approximation to the spectrum $\phi(E)$ is available so that Equation 5.1 can be integrated numerically. It is convenient to define a correction factor F_i for channel i by:

$$\phi_c(E_i) = F_i\,\phi(E_i) \quad , \tag{7.1}$$

where

E_i = energy at the time centre of channel i

$\phi_c(E_i)$ = corrected flux at energy E_i

$\phi(E_i)$ = flux at energy E_i given by Equation 5.2.

The initial flux guess is denoted by the function $k\,\Phi(E)$ where k is a constant which defines the level of the flux. We then have:

$$\phi_c(E_i) = k\,\Phi(E_i) \quad . \tag{7.2}$$

Also, from Equation 5.1:

$$C_i = \frac{N\,A_s\,A_d\,h}{16\pi^2 L^2 r}\; k \iint \Phi(E)\,\epsilon(E)\,\tau_1(E, t' - L/v)\,dE\,dt' \quad , \tag{7.3}$$

and from Equation 5.2:

$$\phi(E_i) = \frac{8\pi^2 L^2 r\,C_i}{N\,A_s A_d\,h\,\epsilon(E_i)\,\tau(E_i)\,E_i\,t_c}$$

$$= \frac{k}{2\,\epsilon(E_i)\,\tau(E_i)\,E_i\,t_c} \iint \Phi(E)\,\epsilon(E)\,\tau_1(E, t' - L/v)\,dE\,dt' \quad ,$$

on substituting for C_i from Equation 7.3. Hence using Equations 7.1 and 7.2:

$$F_i = \frac{\phi_c(E_i)}{\phi(E_i)} = \frac{2\,\epsilon(E_i)\,\tau(E_i)\,E_i\,t_c\,\Phi(E_i)}{\iint \Phi(E)\,\epsilon(E)\,\tau_1(E, t' - L/v)\,dE\,dt'} \tag{7.4}$$

An alternative way to handle Equation 5.1 is to expand the integrand as a Taylor series. Following the procedure used in Section 4 to integrate Equation 4.1 we put:

$$t = t' - L/v$$

$$v = L/(t'-t)$$

$$dE = \frac{2Ev}{L}\,dt \qquad 7.5$$

The integral with respect to E in Equations 4.1 or 5.1 becomes (see Equation 4.2):

$$I = \frac{2}{L}\int_{-h/2\omega_r}^{h/2\omega_r} v\,E\phi(E)\,\epsilon(E)\,\tau_1(E,t)\,dt$$

$$= 2/L\int_{-\infty}^{\infty} v\,E\,\phi(E)\,\epsilon(E)\,\tau_1(E,t)\,dt \qquad 7.6$$

since $\tau_1(E,t)$ is zero for $|t|$ greater than $h/2\omega_r$.

The variables E and v are functions of t and t' so we put:

$$E = E(t,t')$$

$$v = v(t,t') = L/(t'-t)$$

$$X(t,t') = v\,E\,\phi(E)\,\epsilon(E) \qquad 7.7$$

Since $\tau_1(E,t)$ varies slowly with E and rapidly with t, and since it is symmetrical about $t = 0$, we put:

$$\tau_1(E,t) = \tau_1(E_o,t)$$

where $E_o = E(0,t')$

$$v_o = v(0,t') = L/t'$$

Expanding $X(t,t')$ as a Taylor series gives:

$$X(t,t') = X(0,t') + \left(\frac{\partial X}{\partial t}\right)_{t=o} t + \frac{1}{2}\left(\frac{\partial^2 X}{\partial t^2}\right)_{t=o} t^2$$

Since $\tau_1(E_o,t)$ is symmetrical about $t=0$, substitution in Equation 7.6 gives:

$$I = \frac{2}{L}\left[X(0,t')\int_{-\infty}^{\infty}\tau_1(E_o,t)\,dt + \frac{1}{2}\left(\frac{\partial^2 X}{\partial t^2}\right)_{t=o}\int_{-\infty}^{\infty} t^2\,\tau_1(E_o,t)\,dt\right]$$

$$= \frac{2\tau(E_o)}{L}\left[X(0,t') + \frac{1}{2}\left(\frac{\partial^2 X}{\partial t^2}\right)_{t=o} V_b\right]$$

where (compare with Section 6.2):

$$V_b = \frac{\int_{-\infty}^{\infty} t^2\,\tau_1(E_o,t)\,dt}{\int_{-\infty}^{\infty}\tau_1(E_o,t)\,dt} = \frac{\int_{-\infty}^{\infty} t^2\,\tau_1(E_o,t)\,dt}{\tau(E_o)}$$

is the variance of the flight time arising from the width of the neutron burst. If we now put:

$$Y(t') = \tau(E_o)\left[X(0,t') + \frac{1}{2}\left(\frac{\partial^2 X}{\partial t^2}\right)_{t=o} V_b\right] ,$$

substitution in Equation 5.1 gives:

$$C_i = \frac{N A_s A_d h}{16\pi^2 L^2 r} \cdot \frac{2}{L} \cdot \int_{t'_i}^{t'_{i+1}} Y(t')\,dt' \qquad 7.8$$

The time centre T_i of channel i is given by:

$$T_i = 0.5\,(t'_{i+1} + t'_i) ,$$

and $Y(t')$ is expanded about T_i to give:

$$Y(t') = Y(T_i) + \left(\frac{\partial Y}{\partial t'}\right)_{t'=T_i} (t'-T_i) + \frac{1}{2}\left(\frac{\partial^2 Y}{\partial t'^2}\right)_{t'=T_i} (t'-T_i)^2 .$$

Substituting in Equation 7.6 and integrating:

$$C_i = \frac{N A_s A_d h}{16\pi^2 L^2 r} \cdot \frac{2}{L} \cdot t_c\left[Y(T_i) + \frac{1}{2}\left(\frac{\partial^2 Y}{\partial t'^2}\right)_{t'=T_i} V_c\right] , \qquad 7.9$$

where V_c is the flight time variance arising from the timing channel width (Equation 6.10).

Now

$$Y(T_i) = \tau(E_i)\left[X(0,T_i) + \frac{1}{2}\left(\frac{\partial^2 X}{\partial t^2}\right)_{t=o} V_b\right] , \qquad 7.10$$

where E_i is the value of E at $t = 0$ and $t' = T_i$. The corresponding value of v is:

$$v_i = v(0,T_i) = L/T_i , \qquad 7.11$$

so v_i and E_i are the velocity and energy at the time centre of a counting channel. We further assume that the second term in the expression for $Y(T_i)$ is small and that $\tau(E)$ varies slowly with E so we shall have:

$$\left(\frac{\partial^2 Y}{\partial t'^2}\right)_{t'=T_i} = \tau(E_i)\left(\frac{\partial^2 X}{\partial t'^2}\right)_{t'=T_i} . \qquad 7.12$$

Also (see Equations 7.5 and 7.7) since $X(t,t')$ is a function only of $(t'-t)$:

$$\frac{\partial^2 X}{\partial t^2} = \frac{\partial^2 X}{\partial t'^2} = X'' , \qquad 7.13$$

Substituting Equations 7.10, 7.11, 7.12, and 7.13 into 7.9 gives:

$$C_i = \frac{N A_s A_d h}{16\pi^2 L^2 r} \cdot \frac{2}{v T_i} \tau(E_i)\, t_c \left\{X(0,T_i) + \frac{1}{2}\left(\frac{\partial^2 X}{\partial t'^2}\right)_{t'=T_i} (V_b + V_c)\right\} .$$

Comparing this with Equation 5.2 and noting that C_i is proportional to X as far as variation with t' is concerned, the correction factor F_i is given by:

$$F_i = 1 + \frac{1}{2}\,\frac{C_i''}{C_i}\,(V_b + V_c) ,$$

where C_i'' is the second derivative at channel i of the channel counts with respect to flight time.

If the effect on flight time variance of the finite detector height, multiple slits, and flight path uncertainty (see Section 6.2) were included, the above expression would generalize to:

$$F_i = 1 + \frac{1}{2}\,\frac{C_i''}{C_i}\,V_T \qquad 7.14$$

when V_T = total flight time variance.

This form of F_i depends on the second derivative of the counting rate distribution which could be difficult to determine with any accuracy unless very precise values of the channel counting rates were available.

8. DEAD TIME, BACKGROUND, AND AIR ATTENUATION CORRECTIONS

8.1 Introduction

The relation between channel counts and flux was considered in the preceding sections. To obtain the channel counts from the experimentally measured counts it is necessary to make corrections for dead time losses, background, and attenuation by air and aluminium foils in the beam. These corrections are now considered.

8.2 Dead Time Correction

The timing system used with the MOATA chopper can record only one count per timing cycle. If therefore a count is recorded in channel i, no further counts can be recorded during that cycle in channels with greater time delays. Put:

n_T = total number of timing cycles

N_i = observed total number of counts in channel i.

The number of timing cycles unavailable to channel i because of counts in earlier channels is therefore:

$$\sum_{j=1}^{i-1} N_j$$

In addition, a count in channel i prevents the recording of a second count in this channel. Provided the total count in channel i is small compared to n_T, the counts will be randomly distributed in time across the channel, so the average time the channel is closed to a second count is half the channel width. Thus a count in one channel on average renders it only half available to further counts; consequently the total number of timing cycles unavailable to channel i is:

$$\frac{N_i}{2} + \sum_{j=1}^{i-1} N_j$$

If N_i^c is the total number of counts in channel i corrected for dead time losses we have:

$$N_i^c = N_i \,\frac{n_T}{n_T - \left(\frac{N_i}{2} + \sum_{j=1}^{i-1} N_j\right)}$$

$$= \frac{N_i}{1 - \frac{N_i}{2n_T} - \frac{1}{n_T}\sum_{j=1}^{i-1} N_j} \qquad 8.1$$

8.3 Background Correction

There will be a residual counting rate at the detector when the rotor is stationary with the slits closed. This can arise from sources such as a general background of radiation, or leakage of neutrons and gamma rays (if the counter is gamma sensitive) through the rotor. Provided this counting

rate is independent of the angle of rotation of the rotor, it leads to the same background counting rate in each channel. This rate is just the product of the counting rate with slits crossed and the total time per second that a given channel is open to counts. Thus:

$$C_B = \frac{\omega t_c C_s}{\pi} \quad , \qquad 8.2$$

where:

C_B = background counting rate in one channel

C_s = counting rate with slits crossed

ω = angular velocity of the rotor

t_c = time width of counting channel.

In practice C_s could vary slowly during a long run so that it is better to determine C_B simultaneously with the actual experimental run. This can be done because there is a cut-off velocity (Appendix III) below which neutrons are not transmitted by the rotor. This means that there is a maximum flight time for neutrons, so that counts in channels implying greater flight times are a measure of the background. Neutron leakage through the slit walls (Appendix IV) implies that this cut-off velocity is not sharp, but provided measurements are made at sufficiently large time delays the background can be obtained. The most convenient way of measuring at large time delays is to trigger the timing system before the slit opens, and to use the first channels to measure the background. This method was satisfactory when low efficiency BF_3 detectors were used on the MOATA chopper.

If a component of the background is a function of rotor angle, some refinement of the above method is required. This is most likely to happen if a considerable portion of the background arises from leakage through the rotor. Two methods of correcting for this type of component have been used with the MOATA chopper. The first is used in experiments using a Monel metal rotor and high efficiency lithium-glass scintillation detector. This counter is sensitive to gamma-rays and the length of rotor material these have to traverse falls as the slit system nears the open position. In fact

$$\ell_r = 2r - \frac{Nh}{\sin\theta} \quad ,$$

where

ℓ_r = length of rotor material traversed

r = rotor radius

N = no. of slits

h = slit height

θ = angle between the slits and the fully open position.

If c_r is the detector counting rate with the rotor stationary at an angle θ, then c_r will be of the form:

$$c_r = c_o + c \exp(-\Sigma \ell_r) \quad ,$$

where

c_o = constant component of the background

Σ = absorption cross section for the radiations traversing the rotor.

Combining this with the expression for ℓ_r gives:

$$c_r = c_o + c_1 \exp\left(\frac{A}{\sin\theta}\right) \qquad 8.3$$

where c_o, c_1, and A are constants.

In practice the relation (8.3) will only be an approximation since there is a neutron component of the transmitted beam which undergoes multiple scattering in crossing the rotor, so the exponential absorption relation will not be correct. Accordingly the following procedure is used to find c_0, c_1, and A. The form of the relation (8.3) can be found either from the counting rates in the channels before time zero as indicated above (Equation 8.2) for a flat background, or from direct measurements of the counting rate with the rotor stationary and the slit at various angles. In practice the number of channels available before time zero limits the first type of measurement to the range 0° to 30°, whilst the second type would be inaccurate at very small angles because of the difficulty of precise angle measurements in the region where the counting rate is strongly dependent on angle. Because of this, the values of A for a series of assumed values of c_0 are found from the ratio of the counting rates at two angles 90° and about 25°. These values of A and c_0 are used in turn in Equation 8.3 and a least squares fit to the counts in the early channels is made to determine c_1. The values of A and c_0 which lead to a fit over the widest range of channels is then selected. This method gives a satisfactory representation of the background down to angles of about 10°. Below this a hand-drawn curve through the measured distribution in the channels immediately before time zero is used. The background in the channels after time zero is found assuming symmetry about time zero.

In some experiments a stainless steel rotor with a Monel metal slit insert was used. In addition to the above peaking of the background when the slits were nearing the open position, there was also a small peak with the slits at right angles to the open position. This arose because the rotor steel had a very low neutron cross section at about 20 keV. There was therefore a high leakage of neutrons of this energy through the rotor, so the slit insert behaved as a plane absorber rotating in the beam. The slit insert therefore led to a modulated background of the form:

$$c_r = c_0 \left[1 + k \exp\left(-\Sigma t/\sin\theta\right)\right] \qquad 8.4$$

where

c_0, k are constants

Σ = total macroscopic cross section of Monel

t = thickness of Monel slit insert.

In this case the background rise near time zero was confined to rotor angles of up to about 10° so a hand fitted curve was used to correct for it. The value of the constant k which defines the depth of modulation of the background was chosen to give the measured ratio of counting rates with the rotor at angles of 90° and 25°.

8.4 Air and Aluminium Attenuation Correction

Attenuation of the neutron beam by air between the source and the detector will distort the spectrum because the cross section of air is dependent on neutron energy. Consequently as much of the flight path as possible should be evacuated, which entails the use of flight tubes closed by thin aluminium windows at each end. A small correction is also needed for the presence of these windows.

The attenuation of a neutron beam is $\exp(-\Sigma\ell)$ so this correction is:

$$N_i^c = N_i e^{(\Sigma_1 \ell_1 + \Sigma_2 \ell_2)} \qquad 8.5$$

where:

N_i^c = corrected total counts in channel i

N_i = observed total counts in channel i

Σ_1 = total macroscopic cross section of air (cm^{-1})

Σ_2 = total macroscopic cross section of aluminium (cm^{-1})

ℓ_1 = total length of air in the beam

ℓ_2 = total length of aluminium in the beam.

It should be noted that

(i) Corrections have already been made for dead-time and background in N_i.

(ii) The cross section values at an energy corresponding to the time centre of channel i are used. These cross sections vary slowly with energy so do not change appreciably across a channel.

(iii) The cross sections used are the sum of the scattering and absorption cross section since any scattering reaction will remove a neutron from the very narrow beam.

9. GROUPING CHANNELS

In regions of a spectrum where the flux is low, it is often desirable to group channels together to gain an improvement in the statistical accuracy of the channel counting rate measurements. Although the energy resolution is affected this does not matter in many cases, especially at low energies where the resolution is very good.

It can be seen from Equations 4.3 and 5.2 that the quantity given most directly by a chopper measurement is $E\phi(E)$, the flux per unit lethargy which we denote by:

$$\psi(u) = E\phi(E) .$$

It is further noted that in general $\psi(u)$ varies much more slowly than $\phi(E)$, so it is more satisfactory to average $\psi(u)$ over several channels than to try to average $\phi(E)$.

For a single channel $\psi(u_i)$ is really an average over a certain lethargy range, Equation 5.1 defining this average. For the purpose of grouping channels it is assumed that this lethargy range is given by the time width of the counting channel, that is, $\psi(u_i)$ is the average over lethargies between U_i and U_{i+1}, where:

U_i = lethargy corresponding to a neutron of velocity L/t'_i

t'_i = lower time boundary of channel i.

The average flux per unit lethargy over M adjacent channels starting at channel j is now defined as:

$$\bar{\psi}(\bar{u}_m) = \frac{\sum_{i=j}^{j+M-1} \{\psi(u_i) \cdot (U_{i+1} - U_i)\}}{U_{j+M} - U_j} ,$$

where:

$\bar{u}_m$ = mean lethargy of channel group

$= 0.5 (U_{j+M} + U_j)$.

The above average is accurate if $\psi(u)$ is constant or varies linearly with lethargy across a channel. It is also noted that $\bar{u}_m$ is the lethargy at the lethargy centre of the channel group as opposed to u_i which is the lethargy at the time centre of a single channel.

For the above channel group the flux per unit energy is defined as

$$\bar{\phi}(\bar{E}_m) = \frac{\bar{\psi}(\bar{u}_m)}{\bar{E}_m} ,$$

where $\bar{E}_m$ = energy corresponding to $\bar{u}_m$.

10. STATISTICAL ERRORS

In this section the error in $\psi(u_i)$ arising from counting statistics is derived. If the channel counting rate C_i in Equation 5.2 is replaced by the total counts N_i in channel i we have:

N_i = total channel counts obtained in experiment lasting for a total time T_T

and from Equation 5.2:

$$\psi(u_i) = \frac{8\pi^2 L^2 r\, T_i}{N\, A_s A_d\, h\, \epsilon(E_i)\, \tau\,(E_i)\, t_c T_T} N_i$$

$$= k_i N_i \qquad \text{say.}$$

Define the following quantities (see Section 8):

N_i^r = total raw counts in channel i

N_i^d = total counts in channel i after correcting N_i^r for dead time losses

N^b = total background counts per channel

N_i^b = total counts in channel i after correcting N_i^d for background;

then $N_i^b = N_i^d - N^b$

N_i = total counts in channel i after correcting N_i^b for air and aluminium attenuation.

The errors in these quantities are:

$$\delta N_i^r = \sqrt{N_i^r}$$

$$\delta N_i^d = \frac{N_i^d}{N_i^r}\, \delta N_i^r$$

$$\delta N_i^b = \sqrt{(\delta N_i^d)^2 + (\delta N^b)^2}$$

$$\delta N_i = \frac{N_i}{N_i^b}\, \delta N_i^b$$

where it is assumed that errors in the dead time and air attenuation factors are negligible.

Hence:

$$\delta N_i = \frac{N_i}{N_i^b} \sqrt{\left(\frac{N_i^d}{N_i^r}\right)^2 N_i^r + (\delta N^b)^2}$$

$$= \frac{N_i N_i^d}{N_i^b} \sqrt{\frac{1}{N_i^r} + (\delta N^b)^2}$$

and $\delta\psi(u_i) = k_i\, \delta N_i$

If several channels are grouped together (Section 9) the error in the mean flux will be:

$$\delta\bar{\psi}(\bar{u}_m) = \frac{\sqrt{\sum_{i=j}^{j+M-1}\{(U_{i+1}-U_i)\,.\,\delta\psi(u_i)\}^2}}{U_{j+M}-U_j}$$

where the notation is as defined in Section 9.

11. DETERMINATION OF THE POSITION OF TIME ZERO

The position of time zero for neutron flight time measurements occurs when the slit is fully open, and it is necessary to determine the corresponding timing channel. The flight time of γ-rays from the source to the detector is essentially zero, so the position of the zero timing channel can be found by replacing the neutron counter with a γ-ray counter and observing the resulting count distribution.

It is assumed that this distribution is symmetrical about time zero and that it varies linearly with time on either side of zero. Let the count distribution in the three channels nearest to time zero be N_1, N_2, N_3 and assume that these counts are appropriate to the time centres of the channels. Figure 9 shows this count distribution for the two cases which can occur, namely N_1 greater than N_3 and N_1 less than N_3.

Assuming unit channel width, and putting x equal to the delay of time zero after the centre of channel 1 we have from Figure 9

(i) $N_1 > N_3$:

$$\tan\alpha = \frac{N_1}{y} = \frac{N_2}{(x+y)-(1-x)} = \frac{N_3}{(x+y)-(2-x)}$$

$$x = \frac{2N_2-N_1-N_3}{2(N_2-N_3)}$$

(ii) $N_1 < N_3$:

$$\tan\alpha = \frac{N_1}{y} = \frac{N_2}{1+y} = \frac{N_3}{2x+y-2}$$

$$x = \frac{2N_2+N_3-3N_1}{2(N_2-N_1)}$$

The value of x is a function only of the difference of various pairs of counts, so no background corrections are required to N_1, N_2, and N_3.

12. ACKNOWLEDGEMENTS

The aim of this report was to give a complete picture of the methods used to analyse data obtained with the MOATA chopper. These methods have been developed over several years by various members of the Chopper Group and the author wishes to acknowledge this work. In particular, he wishes to acknowledge the work of F. Rocke and Mrs.L. Wall who were responsible for much of the development work and the experimental proving of the techniques used.

13. REFERENCES

Beckurts, K.H., and Wirtz, K. (1964). – Neutron Physics, page 312. Springer-Verlag.

Ellis, P.J. (1964). – A neutron time of flight analyser. AAEC/TM259.

Larsson, K.E., Dahlborg, U., Holmryd, S., Otnes, K., and Stedman, R. (1959). – The slow chopper and time of flight spectrometer in theory and experiment. Arkiv För Fysik Band 16 (19): 199.

Mostovoi, V.I., Pevzner, M.I., Tsitovich, A.P. (1955). – A mechanical velocity selector: Proceedings of the International Conference on the Peaceful Uses of Atomic Energy 4: 12.

Rocke, F.A. (1966). – Neutron spectrometry for a chopper with vanes leakage. A.A.E.C. report in preparation.

Stone, R.S., and Slovacek, R.E. (1956). – Reactor spectrum measurements using a neutron time of flight spectrometer. KAPL1499.

Verbinski, V.V., and Jarrard, J.D. (1961). – Calculation of the transmission function for a neutron chopper, ORNL3193, page 204.

APPENDIX I

RELATION BETWEEN SOURCE STRENGTH AND THE NUMBER OF NEUTRONS CROSSING THE DETECTOR FOR A SINGLE SLIT

In this Appendix, an alternative derivation to that in Section 3 is given for the relation between source strength and number of neutrons crossing the detector for a single fixed slit. It is assumed that the source plane is situated in an isotropic flux ϕ so that each point of the source plane can be regarded as a point source strength $S = \phi/4$ (per unit area), emitting neutrons isotropically in the hemisphere towards the slit and detector.

Set up co-ordinate axes $x' y' z'$ with the z' axis along the axis $0'0$ of the system shown in Figure 10(a) (compare also with Figure 2), the $x'y'$ plane coincident with the source plane, and the y' axis vertical. Consider a point S' at $(x',y',0)$ on the source plane where the source strength per unit area is:

$$S(x',y') = \frac{1}{4}\,\phi(x',y') \quad . \qquad \text{AI.1}$$

Consider first a section in the $x' = 0$ plane. The height $h_y = S_1 S_2$ of the detector which receives neutrons from the point S' on the source is determined by either the slit bounds, as indicated in Figure 10(a), or a combination of this and the detector's bounds as in Figures 10(b) and 10(c). Because of symmetry about the $0'0$ axis, only positions of S' above $0'$ (that is, positive values of y') need be considered, so the following expressions are found for the positions y_1, y_2 of S_1 and S_2:

$$y_1 = \frac{L}{L'}\left(y' - \frac{h}{2}\right) - h/2 \quad , \quad \text{(Figure 10(a))}$$

or $$y_1 = -\frac{h_d}{2} \quad , \qquad \text{if line } S'A' \text{ falls outside the detector CD (Figures 10(b) and 10(c)).}$$

Changing the sign of h/2 gives:

$$y_2 = \frac{L}{L'}\left(y' + h/2\right) + h/2 \quad ,$$

or $$y_2 = \frac{h_d}{2} \quad , \qquad \text{if line } S'A \text{ falls outside the detector CD (Figures 10(b) and 10(c)).}$$

The height h_y is then given by:

$$h_y = y_2 - y_1 \quad .$$

When S' coincides with D', that is, $y' = h_s/2$ (h_s = source height), h_y vanishes.

As y' increases from zero we have two cases:

(i) <u>At $y' = 0$:</u> h_y is determined by detector height (see Figure 10(c)).

If the line $S'C$ passes through the upper slit edge A' when $y' = y'_c$ we have (see Figures 10(c) and 10(b)):

$$h_y = h_d \qquad \text{for } y' < y'_c$$

$$h_y = \frac{h_d}{2} - \frac{L}{L'}\left(y' - \frac{h}{2}\right) + \frac{h}{2} \qquad \text{for } y'_c < y' < \frac{h_s}{2}$$

$$h_y = 0 \qquad \text{for } y' > h_s/2$$

$$y'_c = \frac{h}{2} - \frac{L'}{L}\left(\frac{h_d}{2} - \frac{h}{2}\right) \quad .$$

(continued)

(ii) At $y' = 0$: h_y is determined by slit height (see Figure 10(a)).

If the line S'D passes through the lower slit edge A when $y' = y'_c$ we have (see Figure 10(a) and 10(b)):

$$h_y = y_2 - y_1$$

$$= \frac{h}{2}\left(1 + \frac{L}{L'}\right) \qquad \text{for } y' < y'_c$$

$$h_y = \frac{h_d}{2} - \frac{L}{L'}\left(y' - \frac{h}{2}\right) + h/2 \qquad \text{for } y'_c < y' < h_s/2$$

$$h_y = 0 \qquad \text{for } y' > h_s/2$$

$$y'_c = \frac{L'}{L}\left(\frac{h_d}{2} - \frac{h}{2}\right) - h/2$$

Similar expressions hold for the width h_x of the detector which receives neutrons from the source.

The number of neutrons travelling towards the detector from an area $\delta x' \delta y'$ near (x', y') is:

$$n(x', y') = S(x', y') \frac{h_x h_y}{2\pi(L + L')^2} \delta x' \delta y'$$

and the total number travelling towards the detector is:

$$n = \frac{1}{2\pi(L + L')^2} \iint h_x h_y S(x', y') \, dx' dy' \qquad \text{AI.2}$$

In the case of a uniform source $S(x' y')$ is constant. In case (i) above the integral over y' becomes:

$$\int h_y \, dy' = 2\left[\int_0^{y'_c} h_d \, dy' + \int_{y'_c}^{h_s/2} \left\{\frac{h_d}{2} - \frac{L}{L'}\left(y' - \frac{h}{2}\right) + \frac{h}{2}\right\} dy'\right]$$

and in case (ii):

$$\int h_y \, dy' = 2\left[\int_0^{y'_c} \frac{h}{2}\left(1 + \frac{L}{L'}\right) dy' + \int_{y'_c}^{h_s/2} \left\{\frac{h_d}{2} - \frac{L}{L'}\left(y' - \frac{h}{2}\right) + \frac{h}{2}\right\} dy'\right].$$

In both cases the above expressions reduce to

$$\int h_y \, dy' = h \, h_d \left(\frac{L + L'}{L}\right).$$

A similar expression is obtained for the integral over x' with the slit and detector widths replacing h and h_d. Multiplying the two integrals gives:

$$\iint h_x h_y \, dx' dy' = \frac{(L + L')^2}{L^2} A_s A_d$$

where A_s, A_d are the areas of the slit and detector. We finally obtain using Equations AI.1 and AI.2

$$n = \frac{A_s A_d \phi}{8\pi L^2}$$

which is the same as Equation 3.2.

(continued)

APPENDIX I (continued)

In the case of a non-uniform source the chopper measures a source strength averaged over the source. This average is defined by Equation AI.2 in which h_x and h_y are position dependent weighting factors.

When the rotor is spinning, the slit height h in the equations for h_y becomes time dependent so a further time average must be made. Since the slit transmission probability $[\tau_1(E,t)$ or $\tau'_1(E,t)]$ is proportional to the height of the transmitted neutron beam, this can be substituted for h to give the time variation of h_y, and the average value of h given by:

$$\bar{h}_y \propto \int h_y \, dt$$

where the integral is over one neutron burst. Substitution of the triangular distributions for $\tau_1(E,t)$ or $\tau'_1(E,t)$ given in Section 6.2 leads to the typical form of $\bar{h}_y$ shown in Figure 11. If several slits are present the resultant is the sum of the contributions from the individual slits each of which is slightly displaced from its neighbour. This is illustrated for two slits in Figure 12 which shows that quite complex distributions are possible.

The above discussion is for neutrons of a single energy. The height of the transmitted neutron beam $[\propto \tau_1(E,t)]$ is energy dependent so the spatial width of the weighting factor $\bar{h}_y$ depends on neutron energy. This means that both the size and position of the area of the source scanned by the chopper are energy dependent. If the neutron spectrum is not constant across the whole source area then the beam spectrum measured by the chopper is an average spectrum, the average being different for different energies since $\bar{h}_y$ is energy dependent.

APPENDIX II

SLIT TRANSMISSION PROBABILITY: GENERAL THEORY

In calculating the slit transmission probabilities defined in Section 3, it is assumed that a parallel beam of neutrons is incident on the rotor which has a single slit symmetrically placed about its axis. With (x,y) axes centred on the rotor axis as shown in Figure 13 we consider a neutron with a velocity v moving parallel to the x axis at a height c above it. The equations of motion are:

$$x = v(t'-t) \qquad \text{AII.1}$$

$$y = c \ ,$$

where t' = time

t = time at which neutron crossed the y axis.

If the slit system is parallel to the x axis at time $t' = o$, the slit will be at an angle:

$$\theta = \omega t' \ ,$$

at other times as indicated in Figure 13.

Equations 3.9 and 3.10 define the relative slit transmission probabilities as follows:

$$\tau'_1(E,t) = \frac{2\omega r}{h^2} \int p'(E,t,c)\, dc$$

$$\tau'(E) = \int \tau'_1(E,t)\, dt$$

$$p'(E,t,c) = \exp(-\Sigma \ell) \ .$$

To find $p'(E,t,c)$ it is necessary to calculate the path length ℓ of the neutron in the material of the slit walls. This involves the interaction of two moving objects, the neutron and the slit so it is easiest to consider relative motions only. We therefore set up a co-ordinate system (x', y') with the same origin as the above (x, y) co-ordinates, but fixed to the rotor so that the x' axis is parallel to the slit walls (see Figure 14).

The slit walls are at:

$$y' = \pm s \ ,$$

where the slit height h equals 2s, and they extend between:

$$x' = \pm r \ .$$

This co-ordinate system is at an angle:

$$\theta = \omega t' \ ,$$

to the (x y) axes so that, applying the usual transformation relations and substituting for x and y the neutron equations of motion AII.1, we obtain the equations of motion of the neutron relative to the (x', y') axes, namely:

$$x' = v(t'-t)\cos\omega t' + c.\sin\omega t'$$

$$y' = -v(t'-t)\sin\omega t' + c.\cos\omega t' \qquad \text{AII.2}$$

(continued)

The element of path length $\delta\ell$ of the neutron in the system is given by:

$$(\delta\ell)^2 = (\delta x')^2 + (\delta y')^2$$

$$= [(v + \omega c)^2 + \omega^2 v^2 (t' - t)^2] (\delta t')^2 \quad ,$$

from equations AII.2. Putting:

$$u = \frac{\omega v}{v + \omega c} (t' - t)$$

$$\ell = \frac{(v + \omega c)^2}{\omega v} \int_{u_1}^{u_2} (1 + u^2)^{\frac{1}{2}} du$$

$$= \frac{(v + \omega c)^2}{2 \omega v} \left[\sinh^{-1} u + u (1 + u^2)^{\frac{1}{2}} \right]_{u_1}^{u_2} \quad . \qquad \text{AII.3}$$

Equations AII.2 and AII.3 can be simplified because:

(i) $\omega t'$ is small so that $\sin \omega t' = \omega t'$, $\cos \omega t' = 1$

(ii) u is small so that $\sinh^{-1} u = u$, $u(1 + u^2)^{\frac{1}{2}} = u$

(iii) $v >> \omega c$.

The equations of motion become:

$$x' = v(t' - t) \qquad \text{AII.4}$$

$$y' = -\omega v t'^2 + \omega v t' t + c \quad . \qquad \text{AII.5}$$

Also:

$$u = \omega (t' - t)$$

$$\ell = \frac{v}{\omega} (u_2 - u_1)$$

$$= v (t_2' - t_1') \quad . \qquad \text{AII.6}$$

Equations AII.4 and AII.5 show that the neutron path is a parabola with vertex pointing upwards for ω and v positive. The vertex is situated at the point (see Figure 14):

$$x_v' = \frac{vt}{2} \qquad \text{AII.7}$$

$$y_v' = \frac{\omega v t^2}{4} + c \quad . \qquad \text{AII.8}$$

Change of the sign of t yields a parabola identical to the above except that the apex is at $x' = -x_v'$. This implies symmetry in t, so Equation 3.10 can be written:

$$\tau'(E) = \int_{-\infty}^{\infty} \tau_1'(E, t) \, dt$$

(continued)

$$= 2\int_0^\infty \tau'_2(E,t)\,dt \qquad \text{AII.9}$$

so only positive values of t need be considered.

A typical neutron path through the slit system is shown in Figure 15. In calculating ℓ from Equation AII.6 it can be seen that there are six particular times of interest, namely:

t'_{1L}, t'_{2L} = first and second times of crossing the lower slit plane

t'_{1u}, t'_{2u} = first and second times of crossing the upper slit plane

t'_{IN}, t'_{OUT} = times of entering and leaving the slit system.

The first four times are obtained by putting $y' = \pm s$ in Equation AII.5 to give:

$$y' = -s \qquad t'_{1L}, t'_{2L} = \frac{t \mp \sqrt{t^2 + 4\,\frac{c+s}{\omega v}}}{2} \qquad \text{AII.10}$$

$$y' = +s \qquad t'_{1u}, t'_{2u} = \frac{t \mp \sqrt{t^2 + 4\,\frac{c-s}{\omega v}}}{2} \qquad \text{AII.11}$$

Putting $x' = \pm r$ in Equation AII.4 gives:

$$t'_{IN}, t'_{OUT} = t \mp \frac{r}{v} \qquad \text{AII.12}$$

As c varies there will be a variety of paths in the slit material and these are discussed in the following Appendices.

The effect of off-axis slits can be deduced from the above equations. The boundaries of a slit with its centre line at a distance 'a' above the rotor axis will be at:

$$y' = a \pm s$$

A neutron at a distance (c + a) above the axis will cross the slit boundaries at exactly the same times as one at height c crosses a central slit. Consequently the integral over all c in Equation 3.9 will be the same regardless of the position of the slit. Hence in a multiple slit system the total transmission will be just that of the central slit, times the number of slits, provided the neutrons cross only one slit in passing through the rotor. Neutron paths of interest are only inclined slightly to the slit plane and so will have a considerable length of rotor material to cross if they pass from one slit to another. Accordingly the factor $\exp(-\Sigma\ell)$ in $p'(E,t,c)$ is very small and a neutron has a negligible chance of crossing two slits.

APPENDIX III

SLIT TRANSMISSION PROBABILITY: OPAQUE SLIT WALLS

If the slit walls are completely opaque to neutrons the transmission probability is of the form;

$p'(E,t,c) = 1$ if a neutron does not hit the slit wall

$= 0$ if a neutron hits the slit wall.

For $t > 0$ there are two types of path through the slit as shown in Figure 16. If $t < 2r/v$ the apex of the path (Equation AII.7) is within the slit, otherwise it is outside.

(a) $t < 2r/v$: For the neutron to pass through the slit we must have:

(i) apex of path below upper slit plane so that:

$$y'_v = \frac{\omega v t^2}{4} + c \leqslant s \qquad \text{(Equation AII.8)}$$

$$c \leqslant s - \frac{\omega v t^2}{4} , \qquad \text{AIII.1}$$

(ii) right hand end of path must clear the lower slit plane so that:

$$t'_{2L} \geqslant t'_{OUT} .$$

Hence from Equations AII.10 and AII.11:

$$c \geqslant \omega r t + \frac{\omega r^2}{v} - s. \qquad \text{AIII.2}$$

The above two relations define the upper and lower bounds of the neutron beam which we denote by B_u and B_L.

Hence:
$$\int p'(E,t,c)\,dc = \int_{B_L}^{B_u} dc$$

$$= B_u - B_L$$

$$= 2s - \frac{\omega r^2}{v} - \omega r t - \frac{\omega v t^2}{4} . \qquad \text{AIII.3}$$

This expression (in the range $t \geqslant 0$) is a maximum at $t = 0$. Also for a neutron to pass through the slit:

$$B_u > B_L .$$

To satisfy this inequality at $t = 0$ we must have:

$$v > \frac{\omega r^2}{2s}$$

Since $t = 0$ is the most likely condition for a neutron to be transmitted, this inequality implies that there is a cut-off velocity:

$$v_c = \frac{\omega r^2}{2s} = \frac{\omega r^2}{h} , \qquad \text{AIII.4}$$

below which neutrons cannot cross the slit.

(continued)

Some simplification of expressions obtained later in this Appendix occurs if velocities are defined by the parameter:

$$\beta = \frac{v_c}{v} = \frac{\omega r^2}{2sv} \quad , \qquad \text{AIII.5}$$

which is always less than unity for transmitted neutrons. Using this relation, Equation AIII.3 becomes:

$$B_u - B_L = 2s(1-\beta) - \omega rt - \frac{\omega^2 r^2 t^3}{8s\beta} \quad , \qquad \text{AIII.6}$$

and the condition $t < 2r/v$ becomes:

$$t < \frac{4s\beta}{\omega r} \quad .$$

The expression for $(B_u - B_L)$ vanishes when:

$$t = \frac{4s\beta}{\omega r}\left(\frac{1}{\sqrt{\beta}} - 1\right) \quad ; \qquad \text{AIII.7}$$

(the other root of Equation AIII.6 is excluded because it is greater than $\frac{4s\beta}{\omega r}$). Hence if this value of t is less than $4s\beta/\omega r$ the above expression represents the transmitted burst completely.

The condition for this is:

$$\frac{4s\beta}{\omega r}\left(\frac{1}{\sqrt{\beta}} - 1\right) < \frac{4s\beta}{\omega r} \quad ,$$

$$\beta > \frac{1}{4} \quad .$$

(b) $t > 2r/v$: In this case the criteria for a neutron to pass through the slit are (Figure 16):

(i) path to clear left hand end of upper slit plane:

$$t'_{2u} \leqslant t'_{IN}$$

$$c \leqslant -\omega rt + \frac{\omega r^2}{v} + s \qquad \text{(Equations AII.11 and 12)} \quad ,$$

(ii) path to clear right hand end of lower slit plane:

$$t'_{2L} \geqslant t'_{OUT}$$

$$c \geqslant \omega rt + \frac{\omega r^2}{v} - s \qquad \text{(Equations AII.10 and 12)} \quad .$$

These relations again define the upper and lower bounds of the neutron beam so that:

$$B_u - B_L = 2(s - \omega rt) \quad . \qquad \text{AIII.8}$$

This expression vanishes at:

$$t = \frac{s}{\omega r} \quad .$$

The condition $t > 2r/v$ is equivalent to:

$$t > \frac{4s\beta}{\omega r} \quad .$$

(continued)

APPENDIX III (continued)

The transmission probability of the rotor can now be found from Equations 3.9 and AII.9. These equations are:

$$\tau'_1(E,t) = \frac{2\omega r}{h^2} \int p'(E,t,c)\, dc$$

$$\tau'(E) = 2\int_0^\infty \tau'_1(E,t)\, dt$$

Substituting the above relations (AIII.3, AIII.6, AIII.7) for $\int p'(E,t,c)\, dc$, we obtain the transmission probability for a slit with opaque vanes. This gives on using β as a variable rather than E:

(i) $\beta > \frac{1}{4}$

$$\tau(\beta) = \frac{4\omega r}{h^2} \int_0^{\frac{4s\beta}{\omega r}\left(\frac{1}{\sqrt{\beta}}-1\right)} \left[2s(1-\beta) - \omega rt - \frac{\omega^2 r^2 t^3}{8s\beta}\right] dt$$

$$= \frac{16}{3}\sqrt{\beta} - 8\beta + \frac{8}{3}\beta^2 \qquad \text{AIII.9}$$

(ii) $\beta < \frac{1}{4}$

$$\tau(\beta) = \frac{4\omega r}{h^2}\left\{\int_0^{\frac{4s\beta}{\omega r}} \left[2s(1-\beta) - \omega rt - \frac{\omega^2 r^2 t^2}{8s\beta}\right] dt + \int_{\frac{4s\beta}{\omega r}}^{s/\omega r} 2(s-\omega rt)\, dt\right\}$$

$$= 1 - \frac{8}{3}\beta^2 . \qquad \text{AIII.10}$$

The form of the burst shape given by Equations AIII.6 and AIII.8 is indicated in Figure 17. These are drawn out more accurately in Figure 22 for the cases $\beta = 0.1$ and 0.7. Equations AIII.6 and AIII.8 are valid for positive t only. For negative t replace t by $|t|$ in the equations. The transmission probability $\tau(\beta)$ given by Equations AIII.9 and AIII.10 is shown in Figure 23.

APPENDIX IV

SLIT TRANSMISSION PROBABILITY: TRANSLUCENT SLIT WALLS

The calculation of the slit transmission probability when the slit walls are translucent is essentially the determination of the times t' at which the neutron crosses the slit walls. If this is done for all possible paths through the slit system then the required probabilities can be found using Equations AII.6, 3.9, 3.10, and AII.9.

As noted in Appendix II, because of symmetry, only values of t (the time the neutron passes the rotor axis) greater than zero need be considered. For these values the apex of the neutron path is to the left of the centre of the slit. There are several possible types of path through the slit system depending on the values of t and c (the height of the neutron above the rotor axis). Clearly for c outside a certain range the entire path will be within the material of the slit walls, and the probability of transmission will be in the region exp(−20) in a typical case. This is negligible, so only paths traversing less material than this will be considered in the integration over c.

With these restrictions on c and t there are eight possible types of path through the slit system. These are illustrated in Figure 18 and are considered in detail below. The integral of the transmission probability over a range of c from c_a to c_b for path type i is denoted by:

$$P_i(c_a, c_b) = \int_{c_a}^{c_b} \exp(-\Sigma \ell)\, dc \,, \qquad \text{AIV.1}$$

so that (see Equation 3.9):

$$\tau'_i(E,t) = \frac{2\omega r}{h^2} \Sigma_i P_i(c_{ai}, c_{bi}) \,,$$

where the sum is over all possible path types for a given E and t. Referring to Figure 18 the following values of path length ℓ and $P_i(c_a, c_b)$ are obtained:

(i) Path Type 1

$$\ell = v(t'_{OUT} - t'_{2L})$$

$$= \frac{vt}{2} + r - \frac{v}{2}\sqrt{t^2 + 4\,\frac{c+s}{\omega v}} \qquad \text{(Equations AII.10 and 12).}$$

Put

$$A = \Sigma\left(\frac{vt}{2} + r\right)$$

$$B = -\frac{\Sigma v}{2}\sqrt{t^2 + 4\,\frac{c-s}{\omega v}}$$

Let B_a and B_b denote the values of B when c equals c_a and c_b respectively, then:

$$P_1(c_a, c_b) = \int_{c_a}^{c_b} \exp\,[-(A+B)]\, dc$$

$$= \frac{2\omega}{\Sigma^2 v} e^{-A}\left[e^{-B_a}(1+B_a) - e^{-B_b}(1+B_b)\right] .$$

(ii) Path Type 2

$$\ell = v(t'_{1L} - t'_{IN}) + v(t'_{OUT} - t'_{2L})$$

$$= 2r - v\sqrt{t^2 + 4\,\frac{c+s}{\omega v}} \qquad \text{(Equations AII.10 and 12).}$$

(continued)

APPENDIX IV (continued)

Put

$$A = 2\Sigma_r$$

$$B = -\Sigma_v \sqrt{t^2 + 4\,\frac{c+s}{\omega v}}\ .$$

Let B_a and B_b denote the values of B when c equals c_a and c_b respectively, then:

$$P_2(c_a, c_b) = \int_{c_a}^{c_b} \exp\,[-(A + B)]\ dc$$

$$= \frac{\omega}{2\Sigma^2 v}\, e^{-A}\,[e^{-B_a}(1 + B_a) - e^{-B_b}(1 + B_b)]$$

(iii) Path Type 3

$$\ell = v(t'_{1L} - t'_{IN}) + v(t'_{2u} - t'_{1u}) + v(t'_{OUT} - t'_{2L})$$

$$= 2r - v\sqrt{t^2 + 4\,\frac{c+s}{\omega v}} + v\sqrt{t^2 + 4\,\frac{c-s}{\omega v}} \qquad \text{(Equations AII.10, 11, and 12)}$$

$$P_3(c_a, c_b) = \int_{c_a}^{c_b} \exp(-\Sigma\ell)\ dc\ .$$

This integral has to be evaluated numerically.

(iv) Path Type 4

$$\ell = v(t'_{2u} - t'_{1u}) + v(t'_{OUT} - t'_{2L})$$

$$= \frac{vt}{2} + r - \frac{v}{2}\sqrt{t^2 + 4\,\frac{c+s}{\omega v}} + v\sqrt{t^2 + 4\,\frac{c-s}{\omega v}} \qquad \text{(Equations AII.10, 11, and 12)}$$

$$P_4(c_a, c_b) = \int_{c_a}^{c_b} \exp(-\Sigma\ell)\ dc\ .$$

This integral has to be evaluated numerically.

(v) Path Type 5

$$\ell = v(t'_{2u} - t'_{IN}) + v(t'_{OUT} - t'_{2L})$$

$$= 2r + \frac{v}{2}\left\{\sqrt{t^2 + 4\,\frac{c-s}{\omega v}} - \sqrt{t^2 + 4\,\frac{c+s}{\omega v}}\right\} \qquad \text{(Equations AII.10, 11, and 12)}$$

$$P_5(c_a, c_b) = \int_{c_a}^{c_b} \exp(-\Sigma\ell)\ dc\ .$$

This integral has to be evaluated numerically.

(vi) Path Type 6

$$\ell = v(t'_{2u} - t'_{1u})$$

$$= v\sqrt{t^2 + 4\,\frac{c-s}{\omega v}} \qquad \text{(Equation AII.11)}\ .$$

(continued)

APPENDIX IV (continued)

Put $B = \Sigma_v \sqrt{t^2 + 4\frac{c-s}{\omega v}}$

Let B_a and B_b denote the values of B when c equals c_a and c_b respectively, then:

$$P_6(c_a, c_b) = \int_{c_a}^{c_b} \exp(-B)\, dc$$

$$= \frac{\omega}{2\Sigma^2 v}\left[e^{-B_a}(1 + B_a) - e^{-B_b}(1 + B_b)\right]$$

(vii) Path Type 7

$$\ell = v(t'_{2u} - t'_{IN})$$

$$= r - \frac{vt}{2} + \frac{v}{2}\sqrt{t^2 + 4\frac{c-s}{\omega v}} \qquad \text{(Equations AII 11 and 12)}$$

Put $A = \Sigma\left(r - \frac{vt}{2}\right)$

$$B = \frac{\Sigma_v}{2}\sqrt{t^2 + 4\frac{c-s}{\omega v}}$$

Let B_a and B_b denote the values of B when c equals c_a and c_b respectively, then:

$$P_7(c_a, c_b) = \int_{c_a}^{c_b} \exp\left[-(A + B)\right] dc$$

$$= \frac{2\omega}{\Sigma^2 v} e^{-A}\left[e^{-B_a}(1 + B_a) - e^{-B_b}(1 + B_b)\right]$$

(viii) Path Type 8

$$\ell = 0$$

$$P_8(c_a, c_b) = \int_{c_a}^{c_b} dc = c_b - c_a$$

To find the total integral over c of the transmission probability $p'(E,t,c)$ it is now necessary to determine which $P_i(c_a, c_b)$ are the relevant contributions and the values of the limits c_a and c_b in each case. As c is varied from a large negative to a positive value the type of path changes at certain stages and the limits c_a and c_b are the values of c at which the path type changes. This is illustrated further in Figure 19 for the case where the vertex of the neutron path is outside the slit boundaries ($t > 2r/v$). It is apparent from Figure 19 that there are two possible path sequences through the slits. Initially for a large negative value of c the path is entirely within the material of the slit walls and is therefore of no interest. Increasing c eventually leads to a change to path type 1 when $t'_{2L} > t'_{IN}$ (see Figure 15 for definition of t'_{IN} etc.). Further increase of c leads to two alternatives. If t'_{2L} became larger than t'_{OUT} before t'_{2u} becomes larger than t'_{IN}, path type 8 is obtained (left hand route in Figure 19), otherwise path type 5 is obtained. Path type 7 is obtained when $t'_{2u} > t'_{IN}$ or $t'_{2L} > t'_{OUT}$ respectively in the two cases, and finally the path is entirely within the material of the slit walls when $t'_{2u} > t'_{OUT}$.

There are thus four values of c, namely c_1 to c_4 at which the path types change. These are defined by:

APPENDIX IV (continued)

$$t'_{2L} = t'_{IN} \qquad c_1 = \frac{\omega r^2}{v} - \omega rt - s$$

$$t'_{2L} = t'_{OUT} \qquad c_2 = \frac{\omega r^2}{v} + \omega rt - s$$

$$t'_{2u} = t'_{IN} \qquad c_3 = \frac{\omega r^2}{v} - \omega rt + s$$

$$t'_{2u} = t'_{OUT} \qquad c_4 = \frac{\omega r^2}{v} + \omega rt + s \ .$$

The left hand route in Figure 19 is applicable if c_2 is less than c_3 and the right hand if c_2 is greater than c_3. Thus the integral over c in this case is either:

(a) $c_2 < c_3$

$$\int p'(E,t,c)\,dc = P_1(c_1, c_2) + P_8(c_2, c_3) + P_7(c_3, c_4) \ ,$$

or

(b) $c_2 > c_3$

$$\int p'(E,t,c)\,dc = P_1(c_1, c_3) + P_6(c_3, c_2) + P_7(c_2, c_4) \ .$$

A similar sequence of paths is obtained when the vertex of the neutron path is within the slit system ($t < 2r/v$) but the situation is rather more complicated because of additional alternatives. These are illustrated in Figure 20. In this case there are six positions at which path types change; the above four positions plus two more defined by:

(i) Vertex of neutron path coincides with lower slit plane $\qquad c_L = -s - \frac{\omega vt^2}{4}$.

(ii) Vertex of neutron path coincides with upper slit plane $\qquad c_u = s - \frac{\omega vt^2}{4}$.

The possible groupings of paths and the integration limits are shown in Figure 21 in the form of the flow diagram for preparing the computer programme used to calculate the integral.

The above procedure is used to find $\tau'_1(E,t)$ (Equation 3.9, Figure 19) at several values of t, and a numerical integration with respect to t is then made to obtain the value of the transmission probability $\tau'(E)$.

A comparison of $\tau_1(E,t)$ and $\tau'_1(E,t)$ is given in Figure 22, and of $\tau(E)$ and $\tau'(E)$ in Figure 23. The inverse velocity variable β (Appendix III) is used to represent energy in these figures and the cross section of the material of the slit walls was taken as $1.5\ cm^{-1}$. The sensitivity of $\tau'(E)$ to this cross section is indicated in the following table for Σ in the region of $1.5\ cm^{-1}$

DEPENDENCE OF $\tau'(\beta)$ ON Σ

β	$\frac{d\tau'}{\tau'} \Big/ \frac{d\Sigma}{\Sigma}$
0.1	−0.12
0.2	−0.14
0.5	−0.36
0.7	−0.68
0.9	−1.3
1.0	−1.6
1.2	−3.5

(continued)

APPENDIX IV (continued)

It is possible to test the accuracy of the calculated values of slit transmission probabilities by comparing measurements on the same spectrum at a variety of rotor speeds. This check has been carried out on $\tau'(E)$ by Rocke (1966) who found good agreement with experiment for values of β up to about 0.9.

APPENDIX V

SLIT TRANSMISSION PROBABILITY: AN APPROXIMATION

In Appendix III the transmission probability $\tau(\beta)$ of a slit with opaque walls was derived. It is possible to correct this calculation for neutron leakage through the walls in a very simple manner for values of β less than 0.5.

Consider the calculation of $\tau'(\beta)$ given in Appendix IV where neutron leakage through slit walls is allowed. In the case of β less than about 0.5 the principal contributions to $\tau'(\beta)$ arise from the path groups (see Figures 19–21) which include free passage of neutrons through the slit, that is, which include P_8. Further, since small β implies large v, values of t (the time at which the neutron passes the rotor axis) greater than $2r/v$ will be more important in the integration over t than those between zero and $2r/v$. Thus as a first approximation to allow for neutron leakage we put (see Figure 21):

(i) $t > 2r/v$

$$\int p'(E,t,c)\,dc = P_1(c_1, c_2) + P_8(c_2, c_3) + P_7(c_3, c_4) .$$

(ii) $t < 2r/v$

$$\int p'(E,t,c)\,dc = P_8(c_2, c_u) .$$

Note also that (i) above is the major contribution to $\tau'(\beta)$, so only this expression is considered below:

Using the expressions for P_1, P_7 and c_1 to c_4 given in Appendix IV we find for $P_1(c_1, c_2)$:

$$B_a = -\frac{\Sigma v}{2}\sqrt{t^2 + 4\,\frac{c_1 + s}{\omega v}} = -\frac{\Sigma v}{2}\left(t - \frac{2r}{v}\right)$$

$$B_b = -\frac{\Sigma v}{2}\sqrt{t^2 + 4\,\frac{c_2 + s}{\omega v}} = -\frac{\Sigma v}{2}\left(t + \frac{2r}{v}\right)$$

(note that $t > 2r/v$ and that the positive square root is implied in the expression for B_a).

Hence:

$$P_1(c_1, c_2) = \frac{2\omega}{\Sigma^2 v}\left[e^{-2\Sigma r}\left(1 + \Sigma r - \frac{\Sigma vt}{2}\right) - \left(1 - \Sigma r - \frac{\Sigma vt}{2}\right)\right].$$

Similarly:

$$P_7(c_3, c_4) = \frac{2\omega}{\Sigma^2 v}\left[1 - \Sigma r + \frac{\Sigma vt}{2} - e^{-2\Sigma r}\left(1 + \Sigma r + \frac{\Sigma vt}{2}\right)\right].$$

In practice $\Sigma r \simeq 10$, so $\exp(-2\Sigma r)$ is negligible.

Hence:

$$P_1(c_1, c_2) + P_7(c_3, c_4) = \frac{2\omega t}{\Sigma}$$

Consequently:

$$\begin{aligned}\int p'(E,t,c)\,dc &= P_1 + P_7 + P_8 \\ &= \frac{2\omega t}{\Sigma} + 2(s - \omega r t) \\ &= 2\left[s - \omega t\left(r - \frac{1}{\Sigma}\right)\right] .\end{aligned} \qquad \text{AV.1}$$

(continued)

The corresponding relation for opaque slit walls (Equation AIII.8) is

$$\int p'(E,t,c)\,dc = P_\theta(c_2, c_3)$$
$$= 2(s - \omega rt) \quad .$$

Thus to obtain a first approximation for neutron leakage, the rotor radius in the equation for opaque slit walls is reduced by one mean free path, that is, r is replaced by

$$r' = r - 1/\Sigma \qquad \text{AV.2}$$

To use this result in Equations AIII.9 and AIII.10 for $\tau(\beta)$, it is noted that the modified r value defines a new β value (see Equation AIII.5), namely:

$$\beta' = \frac{\omega r'^2}{2sv} = \frac{\omega(r-1/\Sigma)^2}{2sv} \quad . \qquad \text{AV.3}$$

Use of β' in place of β in Equations AIII.9 and AIII.10 leads to a transmission probability $\tau(\beta')$. These equations are based on Equation 3.9 which is:

$$\tau_1'(E,t) = \frac{2\omega r}{h^2} \int p'(E,t,c)\,dc \quad ,$$

and it is only in the integral of $p'(E,t,c)$ that the modification to r must be made. The use of $\tau(\beta')$ would correspond to a modification in the factor $2\omega r/h^2$ as well. However if we replace Equation 3.9 by:

$$\tau_1'(E,t) = \frac{r}{r'} \frac{2\omega r'}{h^2} \int p'(E,t,c)\,dc \quad ,$$

it is apparent that a first approximation to $\tau'(\beta)$ is:

$$\tau_a(\beta') = \frac{r}{r'} \tau(\beta') \quad . \qquad \text{AV.4}$$

The table below compares the transmission probabilities calculated on these various assumptions, and it can be seen that $\tau_a(\beta')$ is a close approximation to $\tau'(\beta)$ for β values up to 0.5.

Note that $\tau'(\beta)$ and $\tau(\beta')$ depend on Σ as well as β and that Σ varies somewhat with energy. Accordingly the values of Σ and energy used are also included in Table AV.1. These values are a selection from a typical run with the MOATA chopper.

COMPARISON OF TRANSMISSION PROBABILITIES

β	0.01	0.4	0.5	0.6	0.7	0.8	0.9	0.94
E (eV)	191.0	0.168	0.108	0.075	0.055	0.042	0.033	0.031
Σ (cm^{-1})	1.22	1.41	1.44	1.46	1.49	1.51	1.53	1.46
$\tau(\beta)$: Appendix III	1.000	0.598	0.438	0.290	0.170	0.077	0.019	0.007
$\tau'(\beta)$: Appendix IV	1.140	0.811	0.664	0.516	0.382	0.263	0.166	0.147
$\tau_a(\beta')$: Appendix V	1.129	0.801	0.651	0.499	0.362	0.238	0.138	0.113
$\tau'(\beta)/\tau_a(\beta')$	1.01	1.01	1.02	1.03	1.06	1.10	1.21	1.30

APPENDIX VI

EFFECTS OF DETECTOR SIZE AND MULTIPLE SLITS ON TRANSMISSION PROBABILITY

To determine the variance of the neutron flight time arising from the width of the burst transmitted by the slit system (see Section 6.2) we must consider further the effects of finite detector size and multiple slits on the slit transmission probability $\tau_1(E,t)$ (see Appendix III). This Appendix gives a qualitative discussion of this problem, the aim being to obtain a result sufficiently accurate for variance estimates.

The first approximation made is to assume that $\tau_1(E,t)$ can be represented by a triangular function of base width $2T_b$ where (see Section 6.2, Equation 6.8):

$$T_b = 0 \qquad \beta > 1$$

$$= \frac{4s\beta}{\omega r}\left(\frac{1}{\sqrt{\beta}-1}\right) \qquad \frac{1}{4} < \beta < 1$$

$$= \frac{s}{\omega r} \qquad 0 < \beta < \frac{1}{4} \quad .$$

This distribution is for a point detector. With a finite detector it is swept across the detector area which increases the distribution width by a time $2T_s$ (see Section 6.2 and Figure 6) where:

$$T_s = \frac{h_d}{2\omega L} \quad .$$

This process is further illustrated in Figure 24 where the spatial width W_s of the burst from the slit and the detector height h_d are expressed as time widths. The relations between these are:

$$W_s = 2\omega L\, T_b$$

$$h_d = 2\omega L\, T_s \quad .$$

Figure 24 shows that the number of neutrons travelling towards the detector increases steadily as the burst from the slit covers more of the detector, and falls away as the slit burst moves away. If the slit burst width is less than the detector height ($T_b < T_s$) as shown in Figure 24(b), the number of neutrons travelling towards the detector remains constant while the burst from the slit is contained entirely within the detector height, that is, between times $-(T_s - T_b)$ and $+(T_s - T_b)$. If T_b is greater than T_s the number of neutrons travelling towards the detector rises to a peak at time zero and then falls away. It is assumed that the rise and fall of this distribution is linear. This is not strictly true because it is in general quadratic, but the approximation should be sufficient for variance calculations. With this assumption the number of neutrons travelling towards the detector can be represented as shown in Figure 25. These functions are:

(i) $T_s < T_b$

$$f(t) = 0 \qquad |t| > (T_s + T_b)$$

$$= 1 - \frac{|t|}{T_s + T_b} \qquad (T_s + T_b) > |t| > 0 \quad .$$

(ii) $T_s > T_b$

$$f(t) = 0 \qquad |t| > (T_s + T_b)$$

$$= 1 - \frac{|t| - (T_s - T_b)}{2T_b} \qquad (T_s + T_b) > |t| > (T_s - T_b)$$

$$= 1 \qquad (T_s - T_b) > |t| > 0 \quad .$$

(continued)

APPENDIX VI (continued)

With multiple slits the total resultant burst is the sum of N (N equals the number of slits) of the above distributions each displaced in time from its predecessor. As shown in Section 6.2 and Figure 7 the resulting total burst width is $2(T_s + T_b + T_m)$, where :

$$T_m = \frac{H}{2\omega L}$$

In general such a composite burst could have quite a complex shape, as illustrated in Figure 26 for three slits. However, provided T_m is small compared with $T_s + T_b$, as normally happens, it is again reasonable to assume linear rises and falls to the burst and to use the approximate shapes indicated in Figure 26. These are drawn out in more detail in Figure 8.

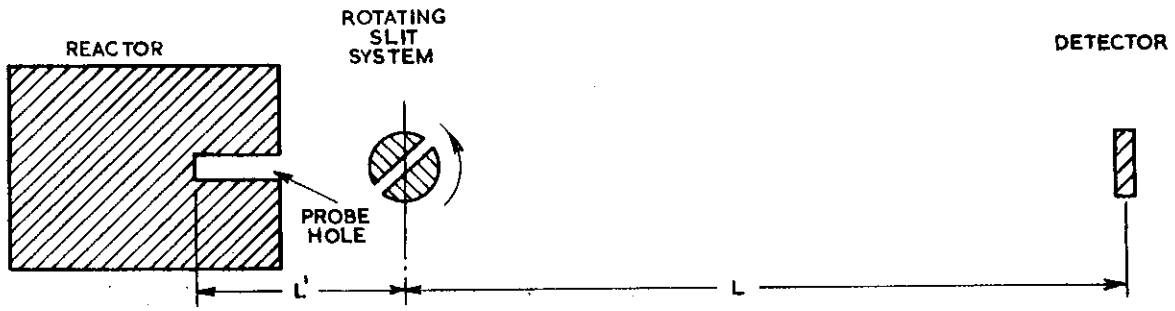

FIGURE 1. OUTLINE ARRANGEMENT OF MOATA CHOPPER

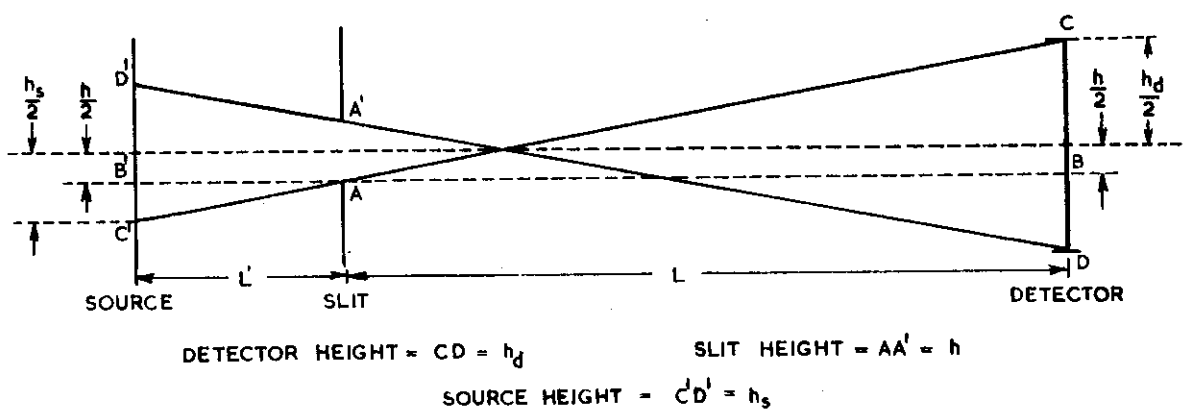

FIGURE 2. SOURCE AREA VIEWED BY THE DETECTOR

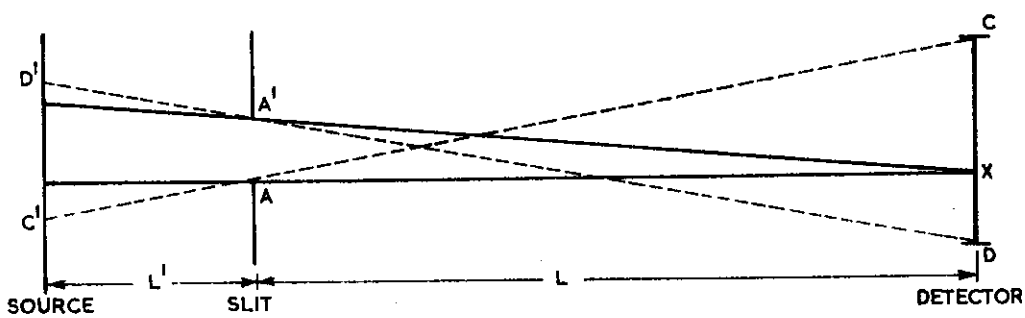

FIGURE 3. SOURCE AREA VIEWED BY A TYPICAL POINT ON THE DETECTOR

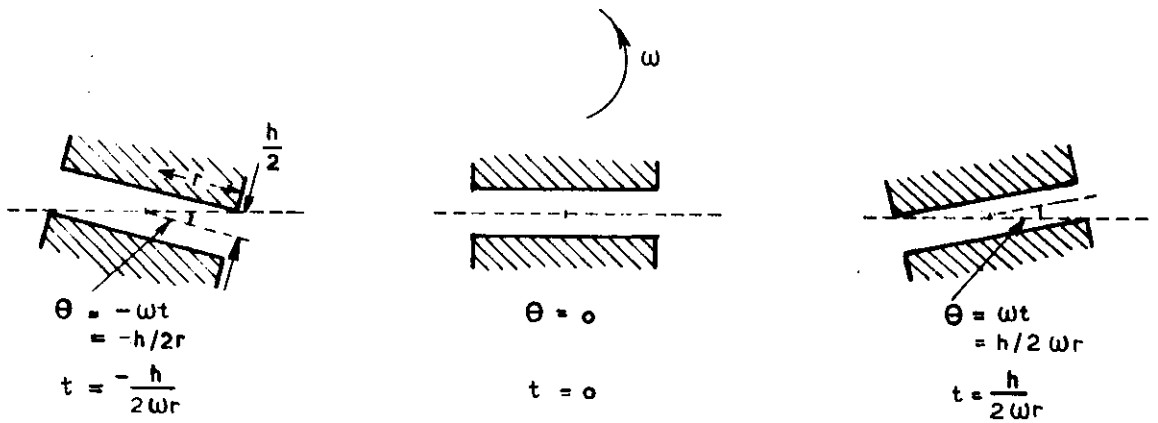

FIGURE 4. SLIT POSITIONS DEFINING BURST WIDTH FOR NEUTRONS WITH INFINITE VELOCITY

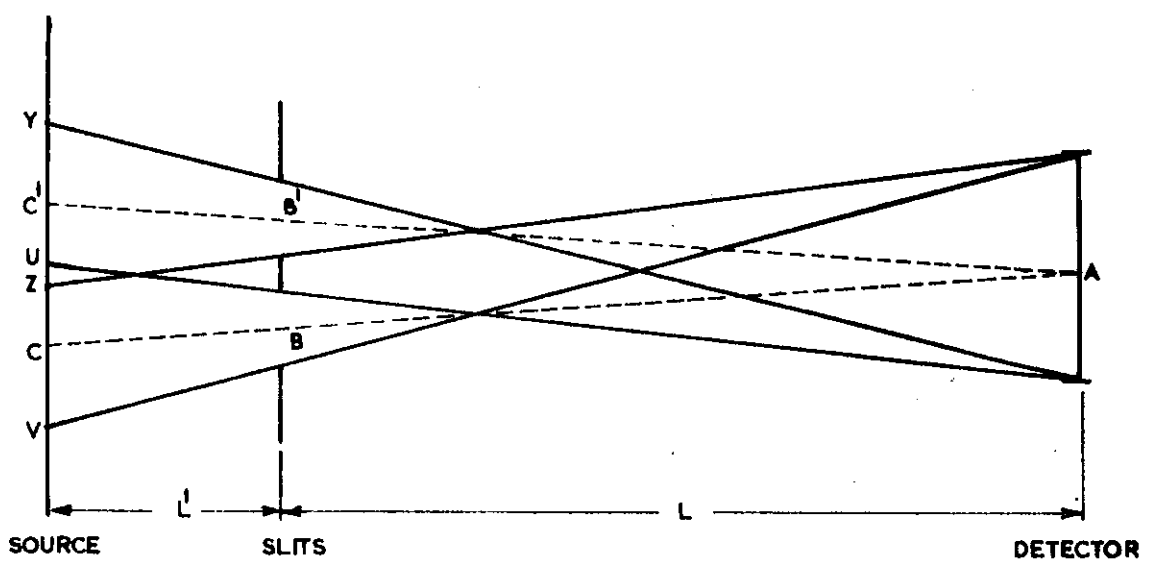

FIGURE 5. SOURCE AREA VIEWED BY THE DETECTOR FOR A ROTOR WITH MULTIPLE SLITS

P1055

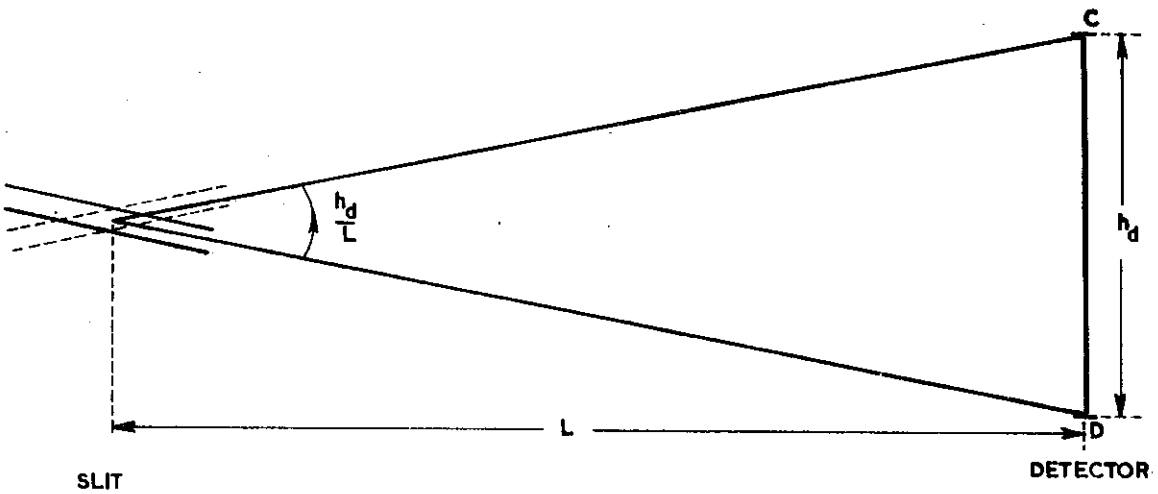

FIGURE 6. CONTRIBUTION OF DETECTOR HEIGHT TO THE VARIANCE OF THE FLIGHT TIME

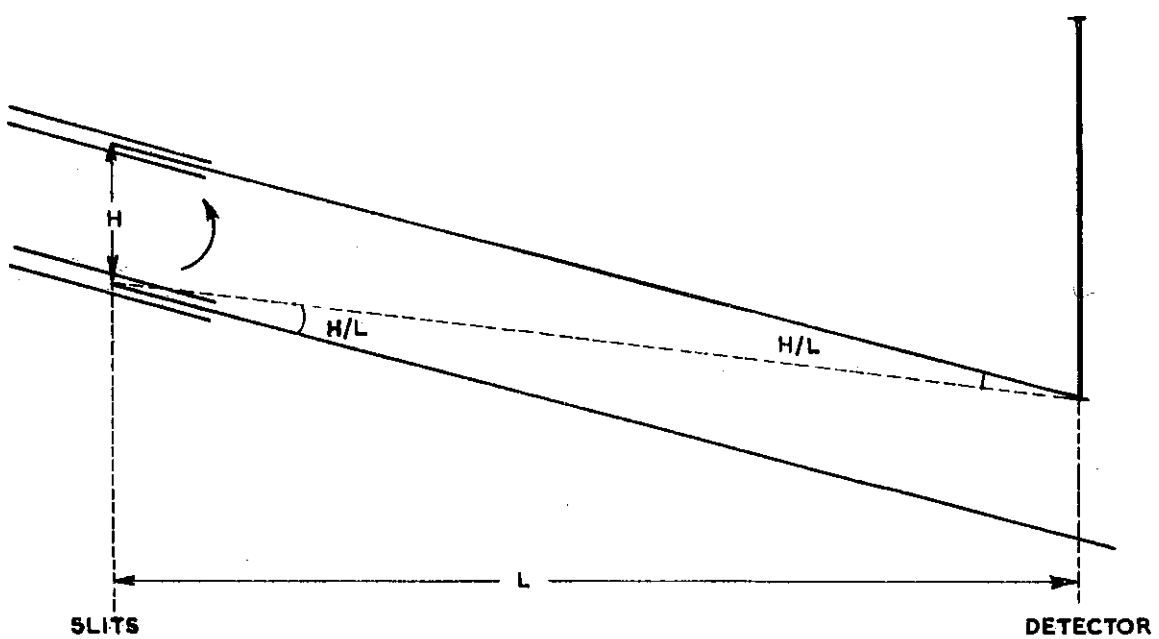

FIGURE 7. CONTRIBUTION OF MULTIPLE SLITS TO THE VARIANCE OF THE FLIGHT TIME

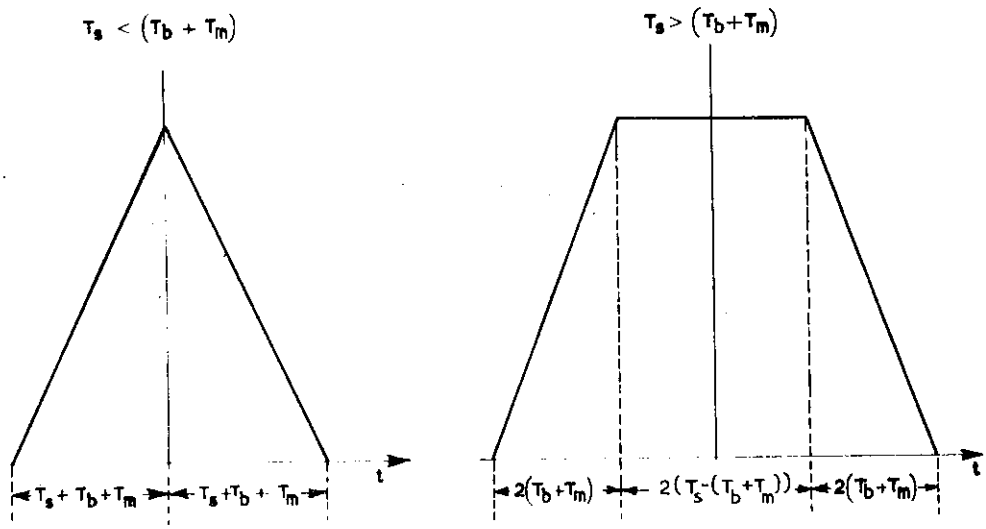

FIGURE 8. APPROXIMATE BURST SHAPES

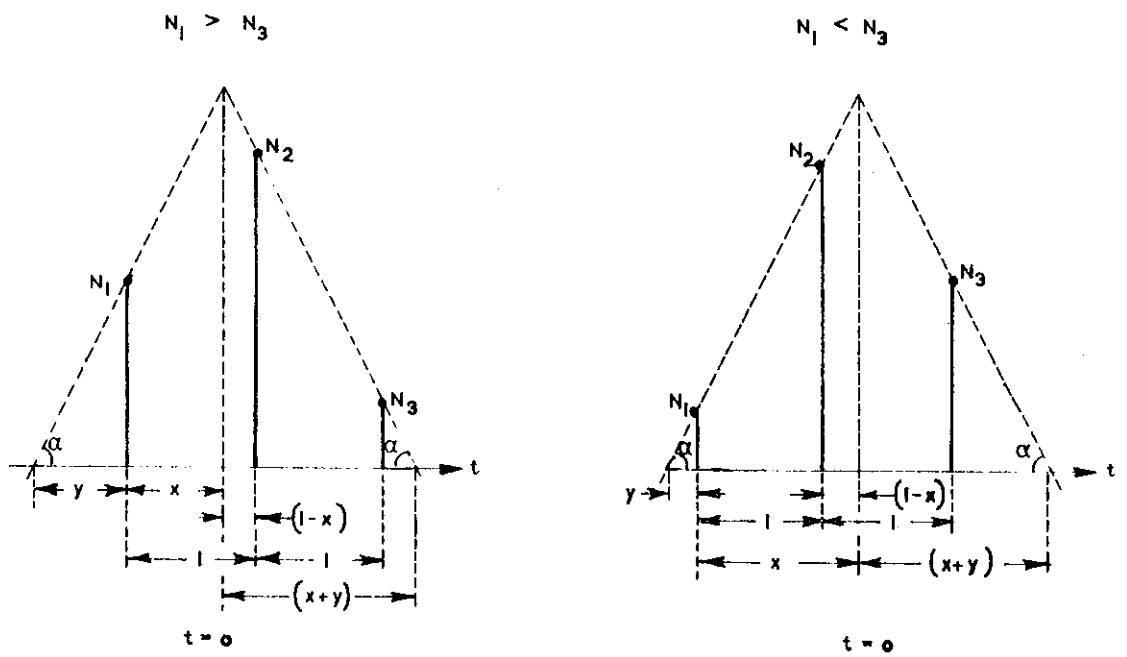

FIGURE 9. APPROXIMATE COUNT DISTRIBUTIONS FOR GAMMA-RAYS

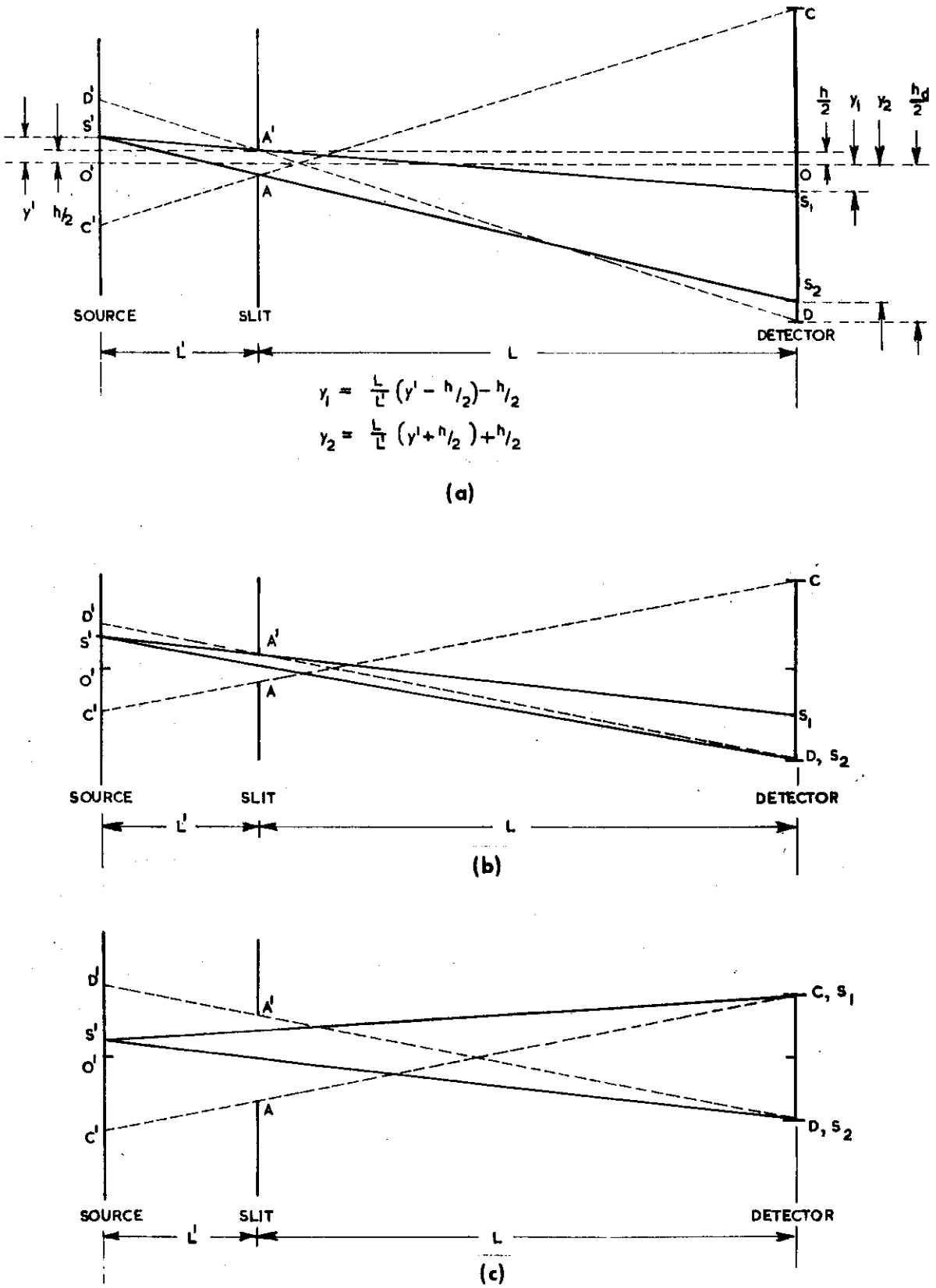

FIGURE 10. DETECTOR AREA RECEIVING NEUTRONS FROM A TYPICAL POINT ON THE SOURCE

PIO 55

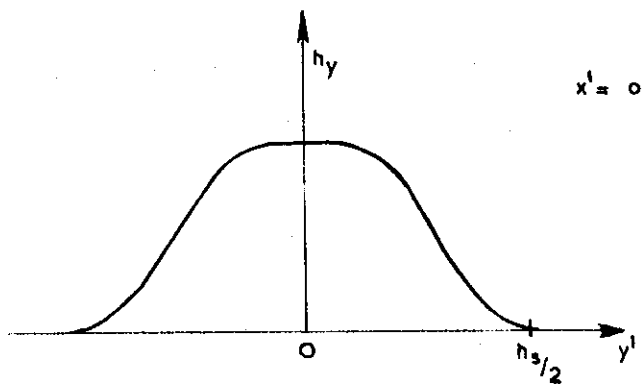

FIGURE 11. SOURCE WEIGHTING FUNCTION FOR ONE SLIT

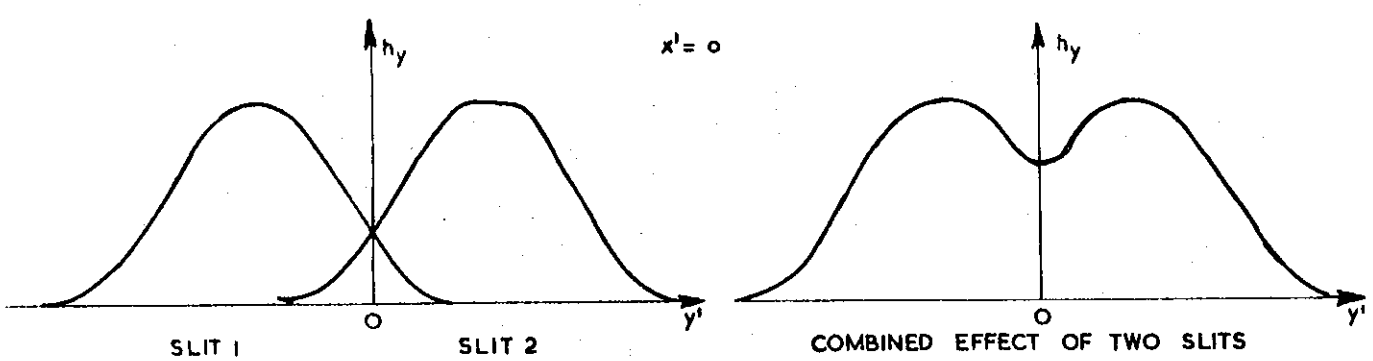

FIGURE 12. SOURCE WEIGHTING FUNCTION FOR TWO SLITS

P1055

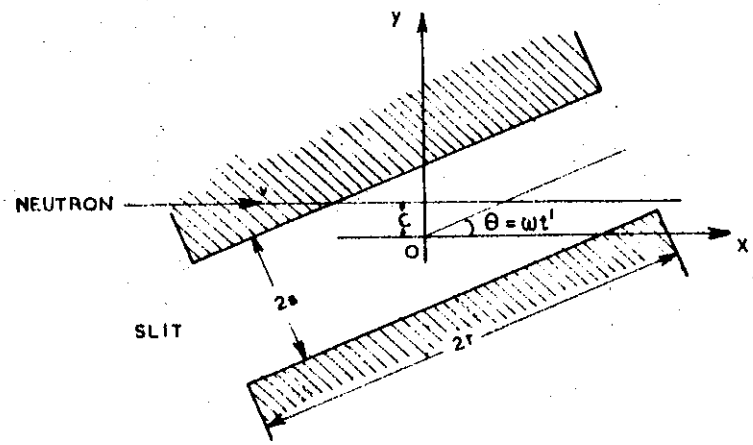

FIGURE 13. LABORATORY COORDINATES

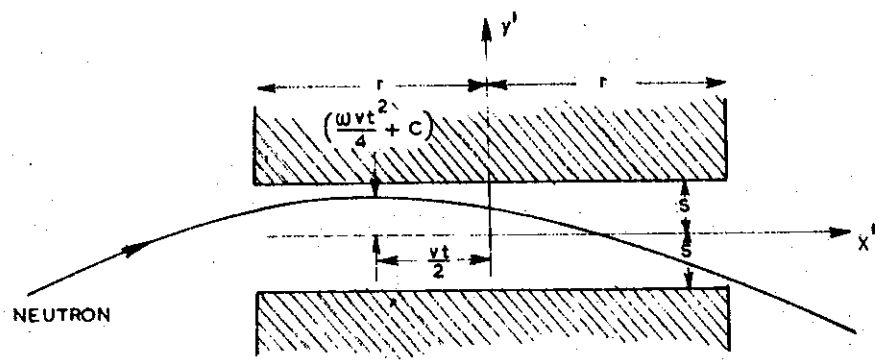

FIGURE 14. SLIT COORDINATES

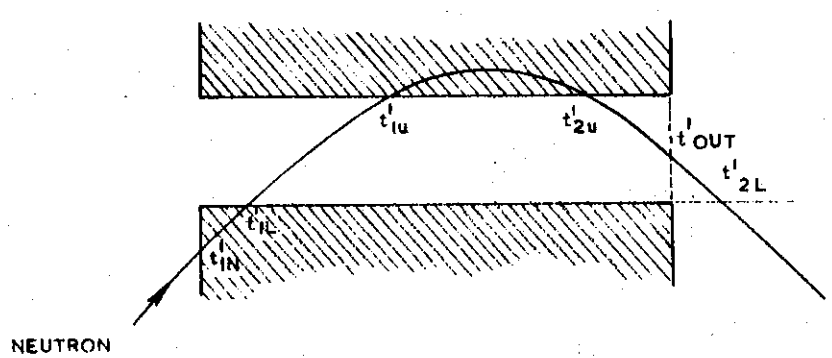

FIGURE 15. TYPICAL NEUTRON PATH THROUGH THE SLIT

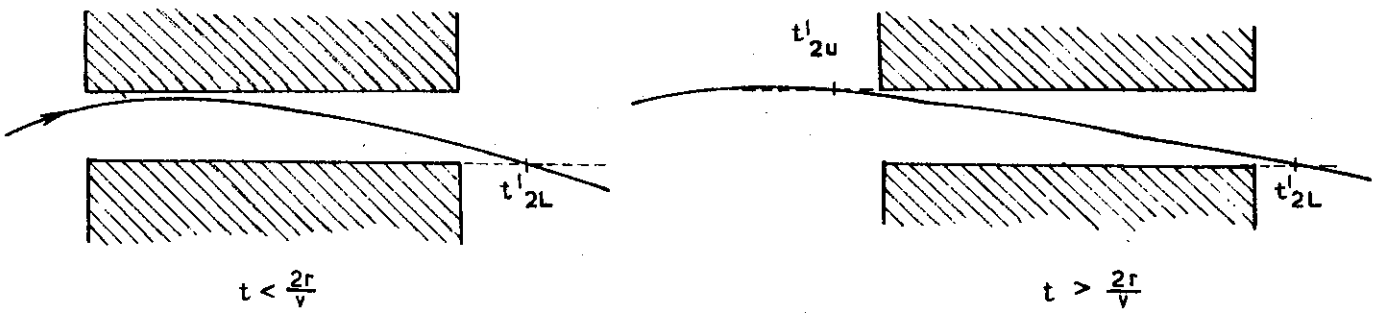

FIGURE 16. TYPES OF PATH THROUGH SLIT WITH OPAQUE WALLS

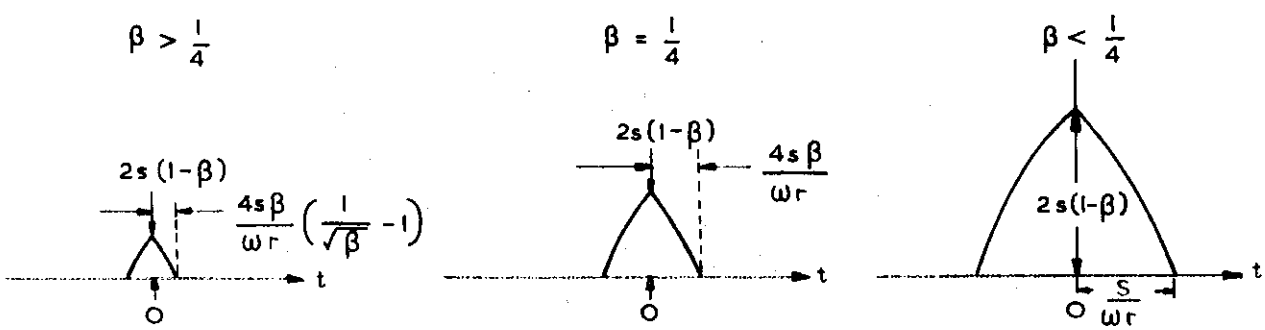

FIGURE 17. HEIGHT OF TRANSMITTED BEAM

P1055

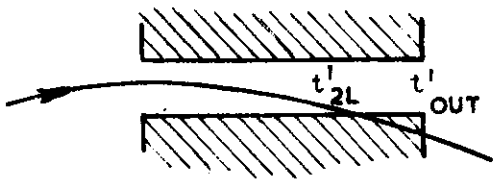

TYPE 1

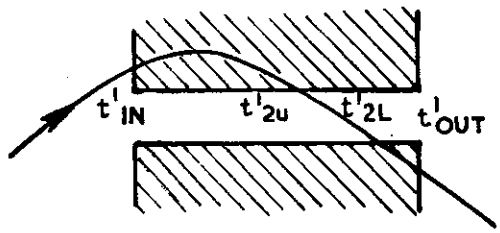

TYPE 5

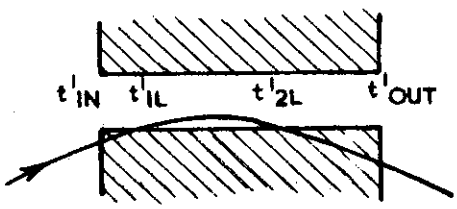

TYPE 2

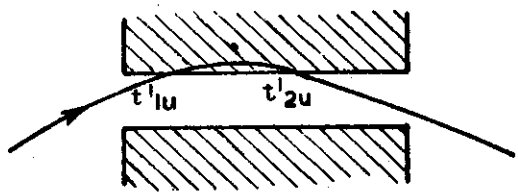

TYPE 6

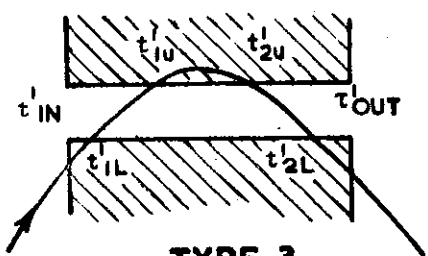

TYPE 3

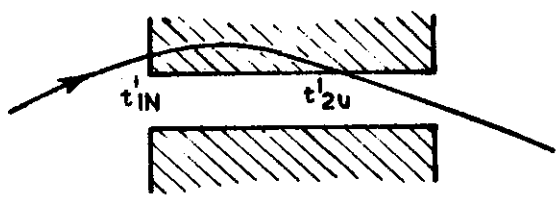

TYPE 7

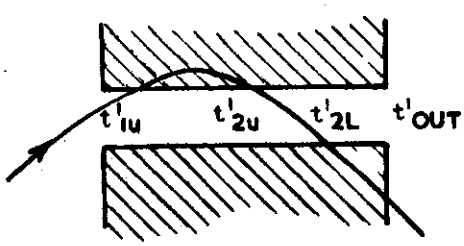

TYPE 4

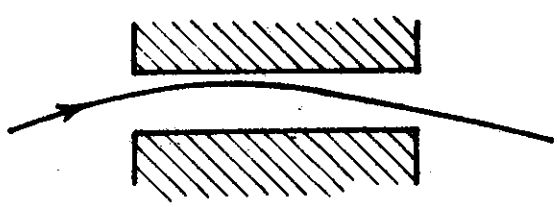

TYPE 8

FIGURE 18. TYPES OF NEUTRON PATHS THROUGH SLIT

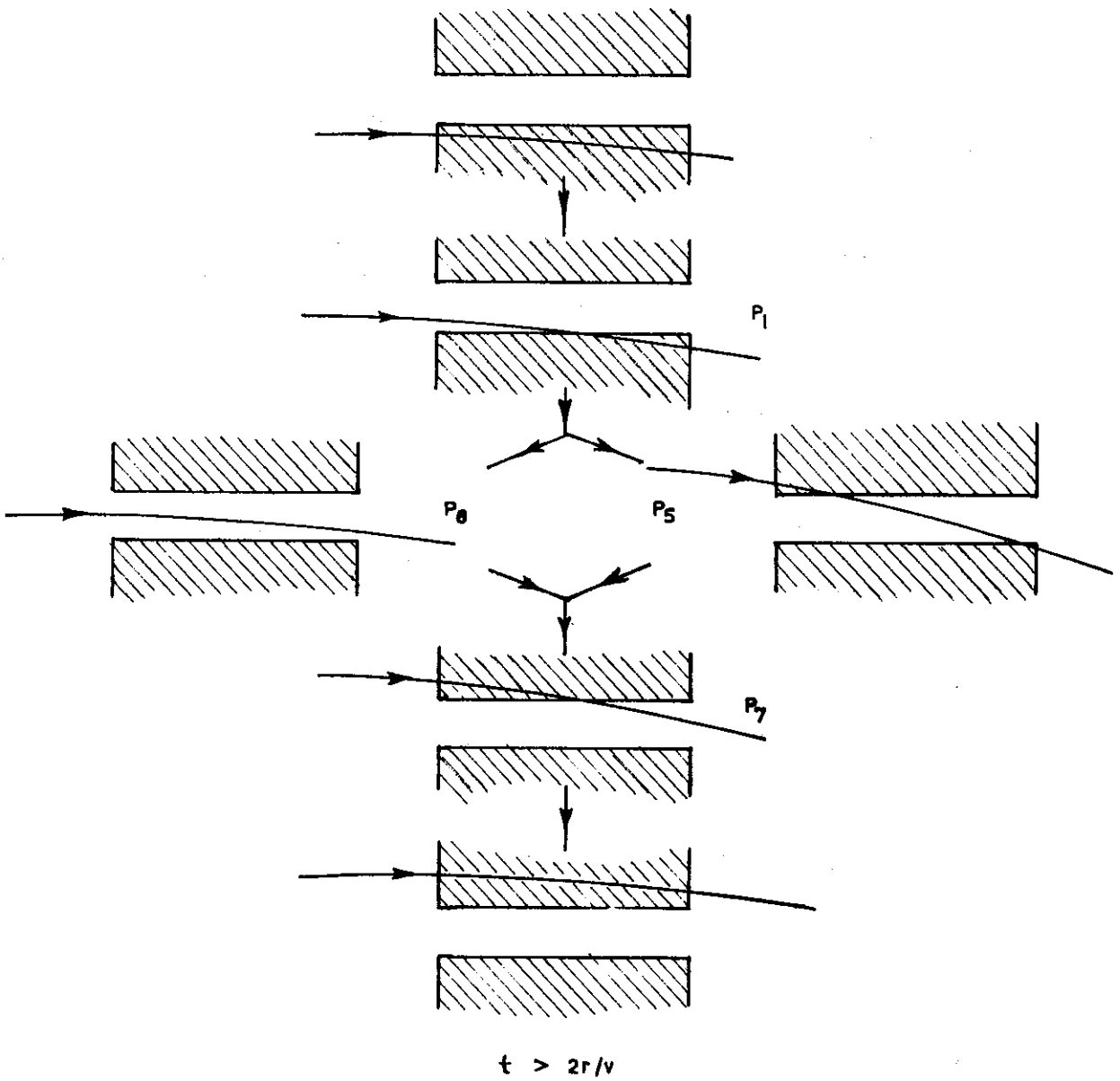

FIGURE 19. NEUTRON PATHS THROUGH SLIT FOR INCREASING c

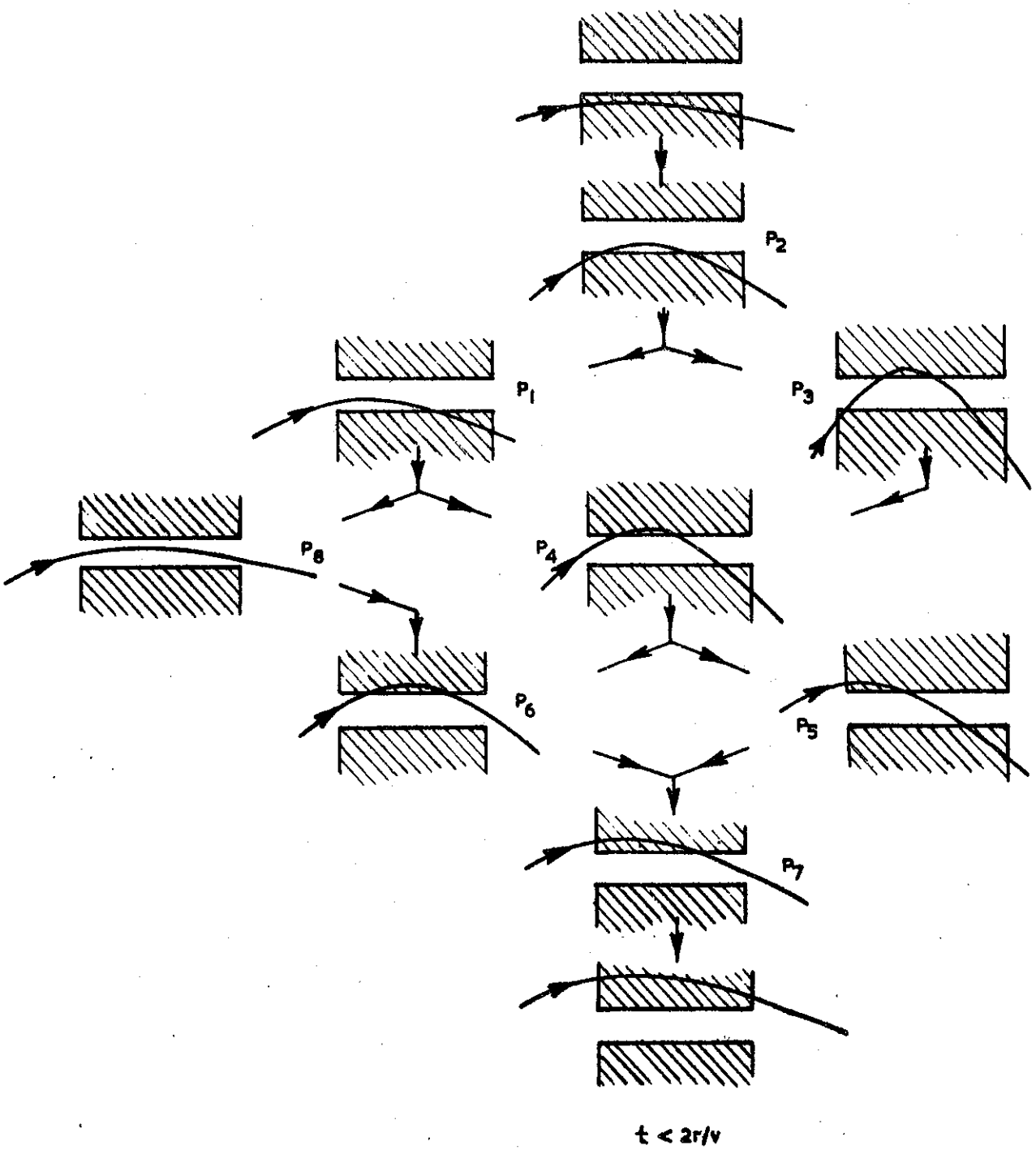

FIGURE 20. NEUTRON PATHS THROUGH SLIT FOR INCREASING c

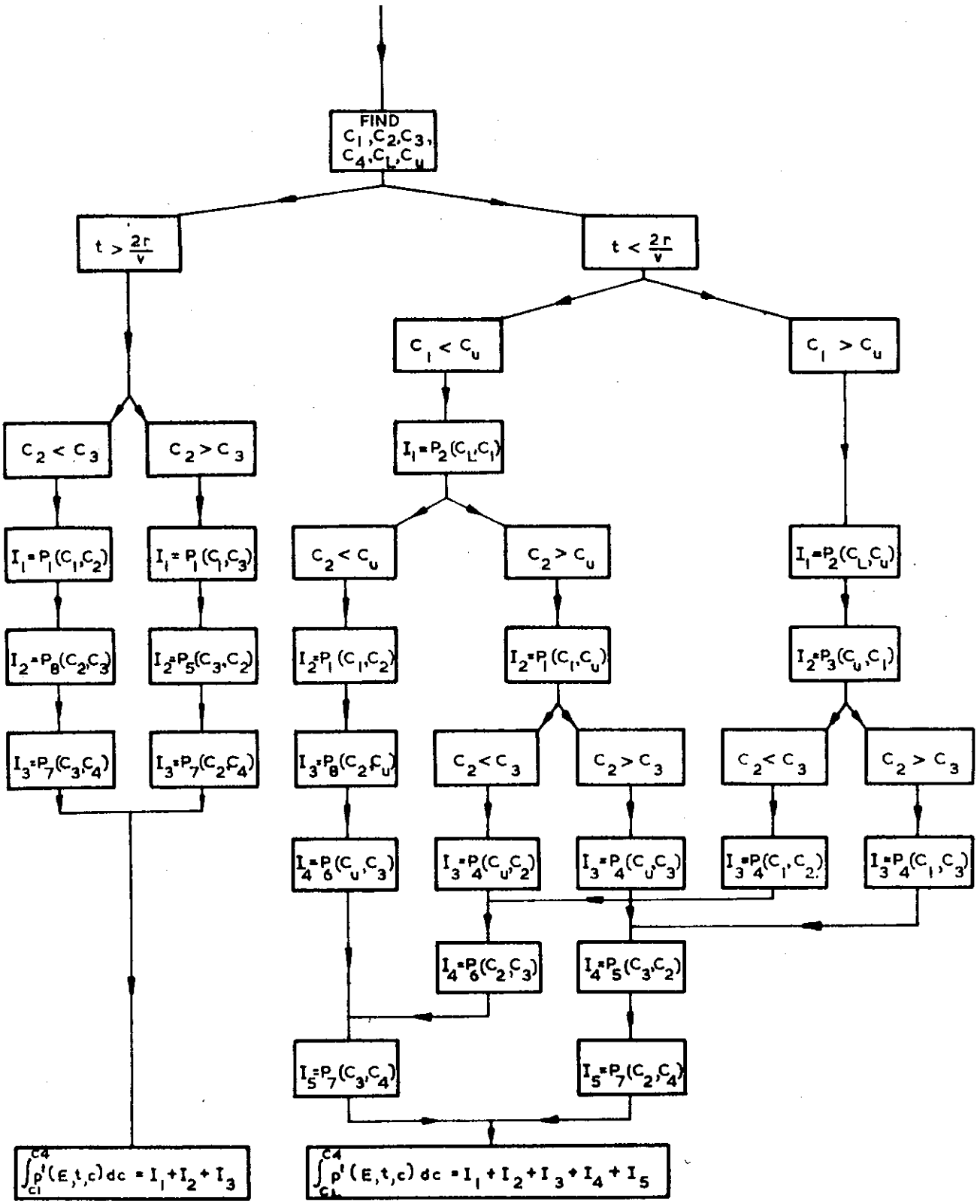

FIGURE 21. CALCULATION OF $\int p'(E,t,c)dc$

P1055

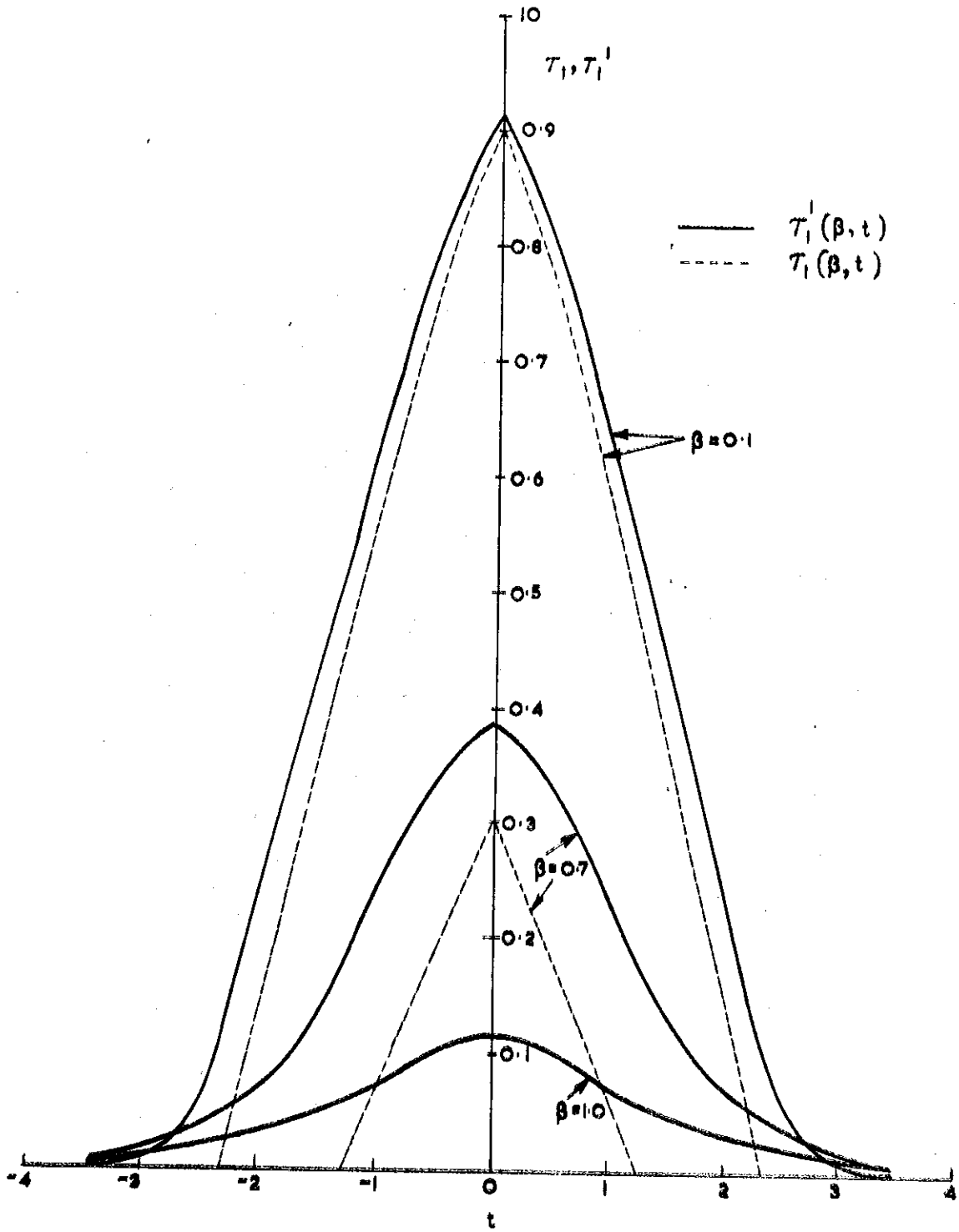

τ_1, τ_1' ARE NORMALIZED TO UNIT SLIT HEIGHT
t IS IN ARBITRARY UNITS

FIGURE 22. COMPARISON OF SLIT TRANSMISSION PROBABILITIES

P1055

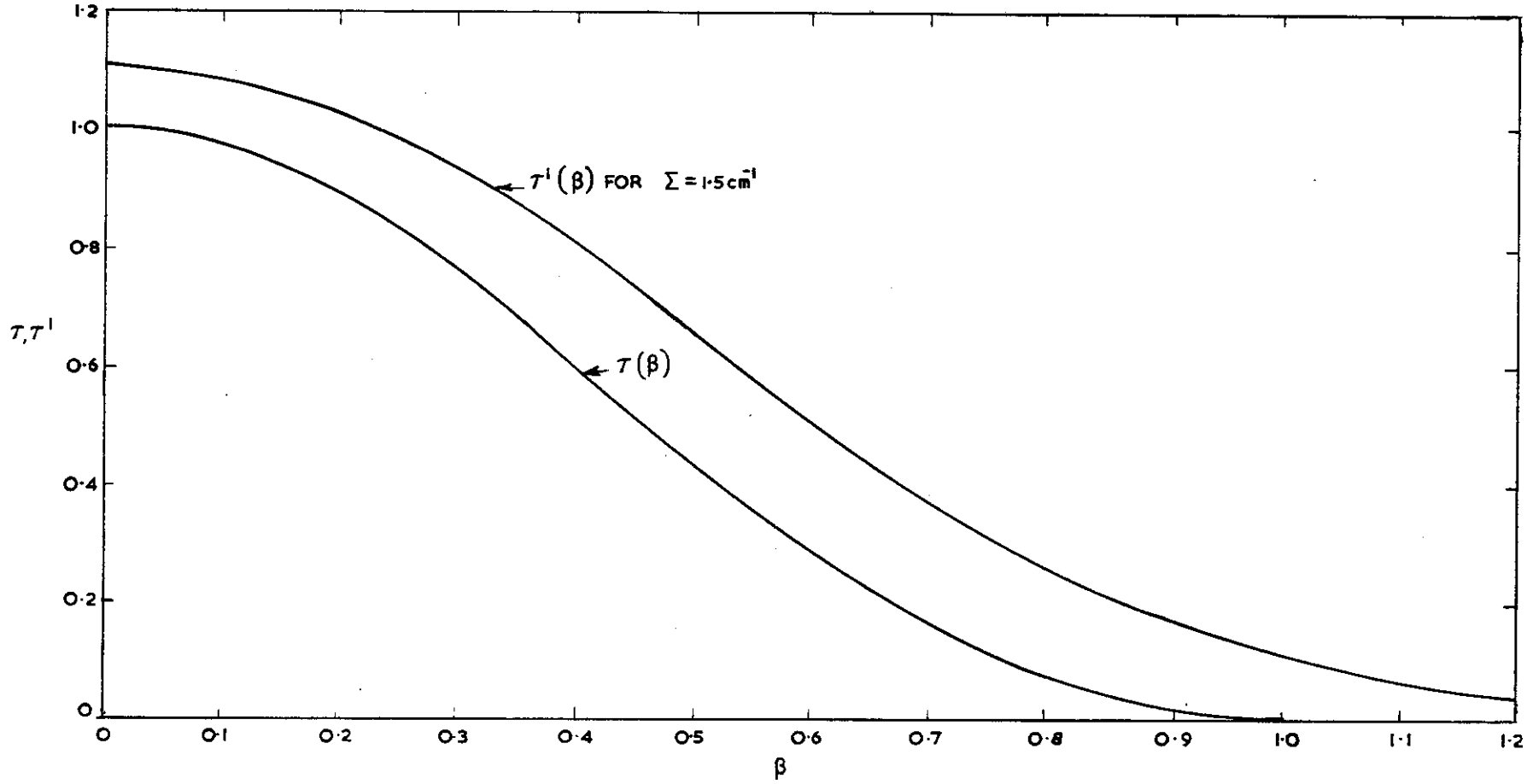

FIGURE 23. SLIT TRANSMISSION PROBABILITIES

P1055

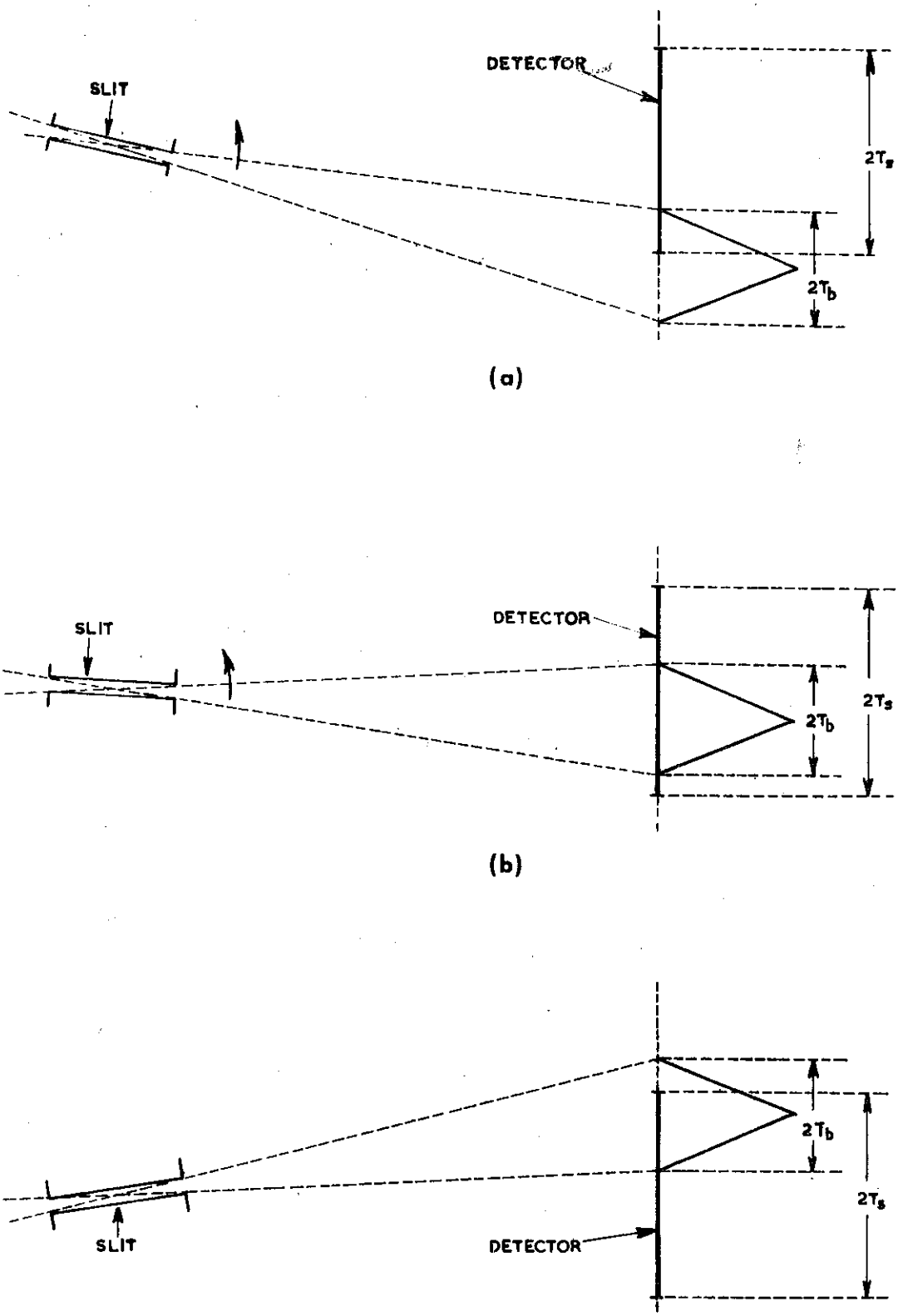

FIGURE 24. TYPICAL POSITIONS OF NEUTRON BURST AS IT IS SWEPT ACROSS THE DETECTOR

P1055

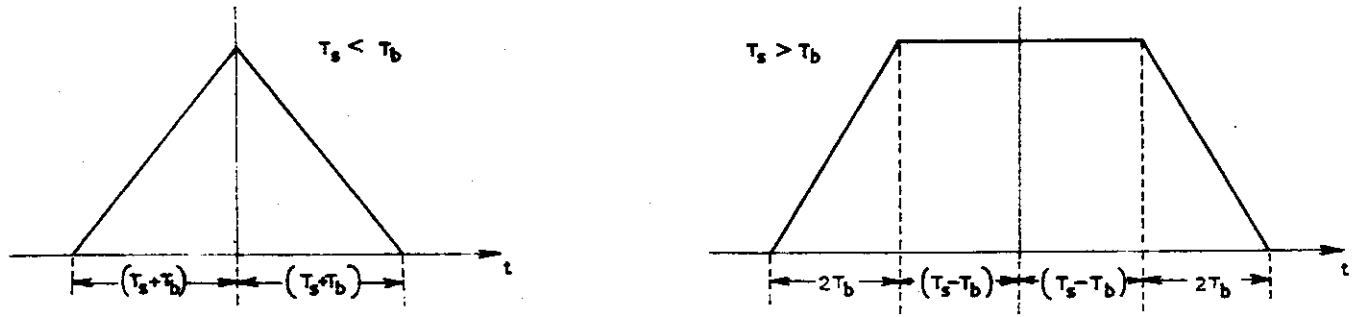

FIGURE 25. TOTAL BURST SHAPE FOR A SINGLE SLIT

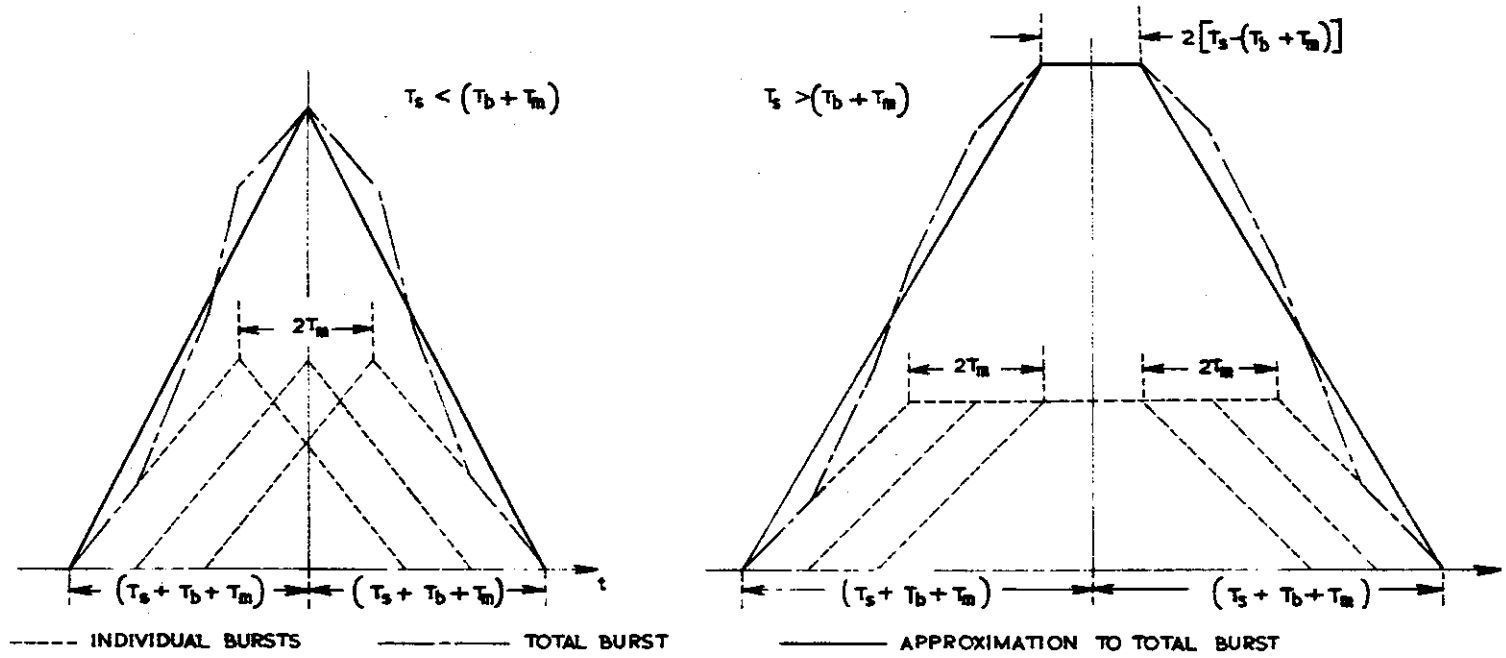

FIGURE 26. FORMATION OF TOTAL BURST SHAPE BY MULTIPLE SLITS